Monthly Notices
of the
ROYAL ASTRONOMICAL SOCIETY

MNRAS **472,** 3337–3353 (2017)
Advance Access publication 2017 August 22

doi:10.1093/mnras/stx2159

Lifetime measurements and oscillator strengths in singly ionized scandium and the solar abundance of scandium

A. Pehlivan Rhodin,[1,2]★ M. T. Belmonte,[3] L. Engström,[4] H. Lundberg,[4] H. Nilsson,[1] H. Hartman,[1,2] J. C. Pickering,[3] C. Clear,[3] P. Quinet,[5,6] V. Fivet[5] and P. Palmeri[5]★

[1]*Lund Observatory, Lund University, PO Box 43, SE-221 00 Lund, Sweden*
[2]*Materials Science and Applied Mathematics, Malmö University, SE-205 06 Malmö, Sweden*
[3]*Physics Department, Blackett Laboratory, Imperial College London, London SW7 2BZ, UK*
[4]*Department of Physics, Lund Institute of Technology, PO Box 118, SE-221 00 Lund, Sweden*
[5]*Physique Atomique et Astrophysique, Université de Mons–UMONS, 20 Place du Parc, B-7000 Mons, Belgium*
[6]*IPNAS, Université de Liège, B15 Sart Tilman, B-4000 Liège, Belgium*

Accepted 2017 August 18. Received 2017 August 18; in original form 2017 July 12

ABSTRACT

The lifetimes of 17 even-parity levels (3d5s, 3d4d, 3d6s and $4p^2$) in the region 57 743–77 837 cm^{-1} of singly ionized scandium (Sc II) were measured by two-step time-resolved laser induced fluorescence spectroscopy. Oscillator strengths of 57 lines from these highly excited upper levels were derived using a hollow cathode discharge lamp and a Fourier transform spectrometer. In addition, Hartree–Fock calculations where both the main relativistic and core-polarization effects were taken into account were carried out for both low- and high-excitation levels. There is a good agreement for most of the lines between our calculated branching fractions and the measurements of Lawler & Dakin in the region 9000–45 000 cm^{-1} for low excitation levels and with our measurements for high excitation levels in the region 23 500–63 100 cm^{-1}. This, in turn, allowed us to combine the calculated branching fractions with the available experimental lifetimes to determine semi-empirical oscillator strengths for a set of 380 E1 transitions in Sc II. These oscillator strengths include the weak lines that were used previously to derive the solar abundance of scandium. The solar abundance of scandium is now estimated to $\log\epsilon_{\odot} = 3.04 \pm 0.13$ using these semi-empirical oscillator strengths to shift the values determined by Scott et al. The new estimated abundance value is in agreement with the meteoritic value ($\log\epsilon_{met} = 3.05 \pm 0.02$) of Lodders, Palme & Gail.

Key words: atomic data – methods: laboratory: atomic – methods: numerical – techniques: spectroscopic – Sun: abundances.

1 INTRODUCTION

The iron-group elements ($21 \leq Z \leq 28$) are produced during supernova type Ia explosions, while supernova type II explosions are responsible for the formation of α-elements such as Mg, Si and S. The even-Z nuclei such as S, Ca, Ti, Cr and Fe have higher cosmic abundance compared to the odd-Z nuclei located in between because of the consecutive capture of α-particles. The production of odd-Z elements is not well understood and does not follow the abundance trends of the α-elements, indicating non-common production mechanisms. In recent years, this has caused an increasing interest in the odd-Z iron-peak elements in astrophysics. Abundance determinations in stars constrain the stellar evolution and supernova explosion models (Pagel 2009). Moreover, transitions from highly excited levels have an additional diagnostic value since they can be used to benchmark non-local thermodynamical equilibrium (NLTE) modelling of stellar atmospheres. Besides the development of 3D hydrodynamic model atmospheres, a trustworthy NLTE treatment is the current challenge for accurate stellar abundances. High-precision atomic data for selected lines are important for this development (Lind, Bergmann & Asplund 2012).

In the case of scandium ($Z = 21$), a realistic 3D NLTE solar atmosphere model has been used by Scott et al. (2015) to revise the solar abundance of scandium resulting in a photospheric value in significant disagreement with the meteoritic abundance (Lodders et al. 2009). Scott et al. (2015) used experimental transition probabilities of five Sc I and nine Sc II lines determined by Lawler & Dakin (1989). The latter authors combined their measured branching fractions with the time-resolved laser induced fluorescence (TR-LIF) lifetimes of Marsden et al. (1988) to obtain absolute A-values for transitions depopulating 51 levels in Sc I and 18 levels in Sc II. In Marsden et al. (1988), only three highly excited even-parity levels of Sc II, belonging to $3d4d\ ^3G$, were measured. Older

★ E-mail: asli.pehlivan@mah.se (APR); patrick.palmeri@umons.ac.be (PP)

lifetime measurements in singly ionized scandium have focused on lower excited odd-parity 3d4p and 4s4p levels (Buchta et al. 1971; Arnesen et al. 1976; Palenius, Curtis & Lundlin 1976; Vogel et al. 1985). On the theoretical side, the most recent calculations of E1 oscillator strengths in Sc II are given in Ruczkowski, Elantkowska & Dembczynski (2014) and Kurucz (2011).

The main goal of this work is to provide a new set of experimental *f*-values for transitions depopulating the highly excited even-parity levels in Sc II, and new calculations for both low- and high-excitation levels and lines. Descriptions of our measurements are presented in Sections 2 and 3. The theoretical method used for the calculation of the radiative parameters is described in Section 4. In Section 5, our results are presented and compared to data available in the literature. The consequence of the proposed set of oscillator strengths on the solar abundance of scandium is discussed in Section 6. Finally, our conclusions are given in Section 7.

2 LIFETIME MEASUREMENTS

The experimental set-up for the two-step Time-Resolved Laser Induced Fluorescence (TR-LIF) measurements at the Lund High Power Laser Facility has been described in detail by Engström et al. (2014) and Lundberg et al. (2016). For an overview, we refer to fig. 1 in Lundberg et al. (2016), and here we give only the most important details. A frequency doubled Nd:YAG laser (Continuum Surelite) with 10 ns pulses was used to produce the free scandium ions by focusing the light on a rotating solid scandium sample in a vacuum chamber with a pressure of around 10^{-4} mbar. The ions in the plasma cone were crossed by two laser beams, a few millimetre above the solid sample, generating the two-step excitations. The fluorescence signal was detected in a direction perpendicular to both the ablation and excitation lasers.

For the first step (4s–4p), we used a Continuum Nd-60 dye laser with either DCM or Pyridine 2 dyes. The 10 ns long pulses were frequency doubled using a KDP crystal, giving the wavelengths needed for the first step. The second laser system excited the final high-energy levels. It consists of a frequency doubled Continuum NY-82 Nd:YAG laser pumping a Continuum Nd-60 dye laser with either DCM or Oxacin dye for wavelengths below or above 660 nm, respectively. The pulse length was reduced from 10 ns to less than 1 ns by stimulated Brillouin scattering. The output was frequency doubled using a KDP crystal and, where higher energy was needed, tripled with a BBO crystal.

For two-step excitation, the timing between the pulses is crucial. For this purpose, a delay generator ensures that the second step is timed to when the population of the intermediate state is at its flat maximum as determined by observing the decay of this level in another channel, see fig. 2 in Lundberg et al. (2016).

The fluorescence emitted by the scandium ions was filtered by a 1/8 m grating monochromator with its 0.28 mm wide entrance slit oriented parallel to the excitation laser beams. This fluorescence light was recorded using a fast micro-channel-plate photomultiplier tube (Hamamatsu R3809U) and digitized using a Tektronix DPO 7254 oscilloscope with 2.5 GHz analogue bandwidth. We used the second spectral order with a 0.5 nm observed line width for all measurements. The excitation laser pulse shape was recorded simultaneously using a fast photo diode and digitized by another channel of the oscilloscope. All decay curves were averaged over 1000 laser pulses and analysed using the DECFIT software (Palmeri et al. 2008) by fitting a single exponential function convoluted by the measured shape of the second-step laser pulse and a background function to the observed decay.

The excitation schemes of the measured Sc II levels are presented in Table 1. This table shows the intermediate levels and their excitation wavelengths, the final levels and their excitation wavelengths from the intermediate levels together with the detection channel level and wavelength. For the levels 4d ^{3}S$_1$, 4d ^{1}D$_2$ and 4p^2 ^{3}P$_2$, it was possible to record the decay in more than one channel. We did not find any differences in the lifetimes obtained from the different channels. Sc II is a complex spectrum with a dense level structure, as shown in Fig. 1. Line blending can be caused by cascades or fluorescence from the intermediate level as discussed by Lundberg et al. (2016). For all measurements, we investigated if there was a line blend affecting the recorded curves. Due to the small spectral width of the laser compared to the energy level separations, we avoid exciting multiple levels.

To investigate any possible saturation effects in the second-step excitation, a set of neutral density filters was placed in the excitation beam. The delay between the ablation and first excitation pulse, the geometrical alignment of the lasers with respect to the target as well as the intensity of the ablation laser were varied to test time-of-flight effects. No systematic effects were observed.

As discussed in Palmeri et al. (2008), the weighting of individual data points, hence the purely statistical uncertainty in the fitted lifetime, is difficult to estimate accurately because the digitizing process is not strictly a counting measurement. However, extensive tests have shown that even for weak lines the dominating factor is the variation between different measurements. The uncertainty in Table 2 represents the uncertainty of 10–20 measurements performed over several days. The difference between subsequent curves is significantly lower than the quoted uncertainty, usually less than 1 per cent.

3 BRANCHING FRACTION MEASUREMENTS

A water-cooled hollow cathode discharge lamp (HCL) was used to produce the free scandium ions. The lamp has an iron cathode with anodes on each side, separated by glass cylinders. A small piece of scandium was placed in the cathode. We used argon, with a pressure of 0.3 Torr, as a buffer gas and applied currents ranging from 0.2 to 0.5 A. These measurements at different currents are very important to find and compensate for self-absorption effects. If self-absorption is not treated correctly, the measured relative line intensity may be less than the true intensity of the line. This in turn changes the branching fraction that is essential to derive oscillator strengths. Self-absorption was observed in the case of the 3d4d ^{3}D$_3$, 3d4d ^{3}S$_1$ and 3d4d ^{3}P$_2$ levels, and the affected lines were corrected. More details on this procedure can be found in Pehlivan, Nilsson & Hartman (2015).

The spectra were recorded with the vacuum ultraviolet Fourier transform spectrometer (VUV FTS) at the Blackett Laboratory, Imperial College London (Pickering 2002) in the interval 23 500–63 100 cm^{-1} (425–158 nm) using a resolution of 0.039 cm^{-1}. We used two different photomultiplier tube detectors: Hamamatsu R7154 and R11568, the latter with a UG5 filter. Each scandium measurement consists of 12 co-added scans. To determine the relative response functions of the system, we used standard lamps: a tungsten filament lamp (800–300 nm) and a deuterium lamp (410–116 nm) for the wavelength region (425–210 nm), and a deuterium standard lamp alone for the region (317–158 nm). The tungsten lamp was calibrated by the UK National Physical Laboratory

Table 1. Measured Sc II levels and the corresponding two-step excitation schemes.

Final	First-step excitation			Second-step excitation			Detection	
level[a]	Starting level[a] (cm^{-1})	Intermediate level[a] (cm^{-1})	λ_{air} (nm)	Final level[a] (cm^{-1})	λ_{air} (nm)	Scheme[b]	Lower level[a] (cm^{-1})	λ_{air} (nm)
$5s\ ^3D_3$	67.72	27 602.45	363.07	57 743.92	331.67	2ω	27 841.35	334.32
$5s\ ^1D_2$	67.72	27 602.45	363.07	58 252.09	326.17	2ω	32 349.98	385.96
$4d\ ^1F_3$	177.76	29 823.93	337.22	59 528.42	336.55	2ω	26 081.34	298.89
$4d\ ^3D_1$	177.76	29 823.93	337.22	59 875.08	332.67	2ω	27 917.78	312.83
$4d\ ^3D_2$	177.76	29 823.93	337.22	59 929.46	332.07	2ω	28 021.29	313.31
$4d\ ^3D_3$	177.76	29 823.93	337.22	60 001.91	331.27	2ω	28 161.17	313.97
$4d\ ^3G_3$	177.76	29 823.93	337.22	60 267.16	328.39	2ω	27 443.71	304.57
$4d\ ^1P_1$	177.76	29 823.93	337.22	60 400.41	326.95	2ω	26 081.34	291.30
$4d\ ^3S_1$	177.76	29 823.93	337.22	61 071.43	319.93	2ω	29 823.93	319.93
							39 345.52	460.15
$4d\ ^3F_2$	2540.95	32 349.98	335.37	63 374.63	322.23	2ω	27 917.78	281.95
$4d\ ^3F_4$	2540.95	32 349.98	335.37	63 528.54	320.64	2ω	28 161.17	282.66
$4d\ ^1D_2$	2540.95	32 349.98	335.37	64 366.68	312.25	2ω	26 081.34	261.12
							30 815.70	297.97
$4d\ ^3P_2$	2540.95	32 349.98	335.37	64 705.89	308.98	2ω	29 823.93	286.60
$4p^2\ ^1D_2$	177.76	28 161.17	357.25	74 433.30	216.04	3ω	32 349.98	237.55
$4p^2\ ^3P_1$	177.76	29 823.93	337.22	76 360.80	214.82	3ω	39 345.52	270.08
$4p^2\ ^3P_2$	177.76	29 823.93	337.22	76 589.30	213.76	3ω	28 161.17	206.43
							39 115.04	266.77
							39 345.52	268.42
$6s\ ^3D_3$	177.76	29 823.93	337.22	77 387.17	210.18	3ω	28 161.17	203.08

Notes. [a]All energy-level values and wavelength values are from Johansson & Litzén (1980).
[b]2ω and 3ω stand for, respectively, frequency doubling and tripling excitation schemes. All first-step levels are excited using a frequency doubling scheme (2ω).

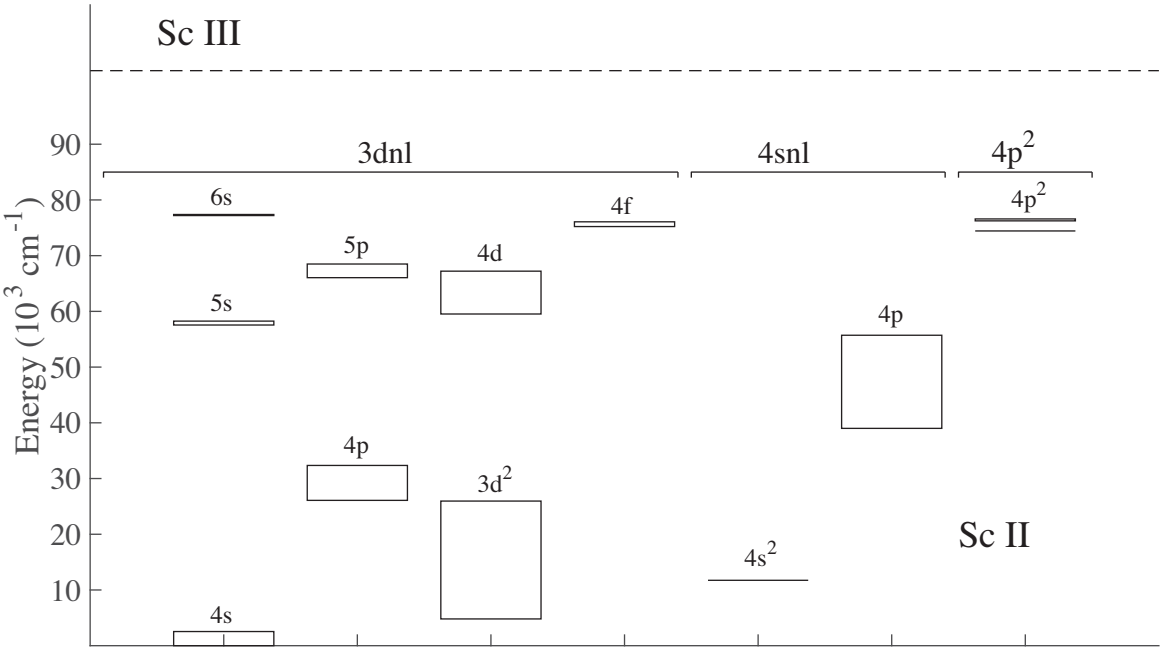

Figure 1. Partial energy level diagram of Sc II, the energy level values are from Johansson & Litzén (1980). Each box consists of several levels.

and the deuterium lamp by Physikalisch-Technische Bundesanstalt, in Berlin. In the region where the lamps overlap, the response functions were placed on the same relative scale. We recorded the spectrum of the calibration lamps immediately before and after each scandium measurement. The HCL and the calibration lamps were placed at the same distances from the FTS, and a mirror was used to select the light source without moving the lamps.

In astrophysics, oscillator strengths (*f*-values) or log (*gf*) values are the parameters used for abundance analysis. The *f*-value is proportional to the transition probability for E1 transitions by

$$f = \frac{g_u}{g_l}\lambda^2 A_{ul} 1.499 \times 10^{-16}, \quad (1)$$

Table 2. A comparison of radiative lifetimes (τ) in Sc II.

Level[a]	E^a (cm^{-1})	$\tau^b_{\text{this cal}}$ (ns)	$\tau^c_{\text{this exp}}$ (ns)	$\tau_{\text{other exp}}$ (ns)	$\tau_{\text{other cal}}$ (ns)
3d4p $^1D^o_2$	26 081.34	6.65		7.5 ± 0.4^d	6.54^i
				7.16 ± 0.18^e	7.79^j
				7.8 ± 0.8^h	
3d4p $^3F^o_2$	27 443.71	5.68		6.2 ± 0.3^d	5.38^i
				6.2 ± 0.2^f	5.90^j
				6.5 ± 0.4^g	
3d4p $^3F^o_3$	27 602.45	5.62		6.1 ± 0.3^d	5.32^i
					5.83^j
3d4p $^3F^o_4$	27 841.35	5.54		6.1 ± 0.3^d	5.24^i
				5.6 ± 0.6^h	5.75^j
3d4p $^3D^o_1$	27 917.78	4.44		4.7 ± 0.2^d	4.20^i
				4.61 ± 0.10^e	4.67^j
3d4p $^3D^o_2$	28 021.29	4.41		4.7 ± 0.2^d	4.17^i
				4.66 ± 0.14^e	4.64^j
3d4p $^3D^o_3$	28 161.17	4.38		4.7 ± 0.2^d	4.15^i
				4.55 ± 0.15^e	4.59^j
				6.1 ± 0.6^h	
3d4p $^3P^o_0$	29 736.27	6.36		7.7 ± 0.4^d	6.80^i
				7.48 ± 0.18^e	7.44^j
3d4p $^3P^o_1$	29 742.16	6.39		7.6 ± 0.4^d	6.76^i
				7.3 ± 0.3^e	7.45^j
3d4p $^3P^o_2$	29 823.93	6.30		7.4 ± 0.4^d	6.67^i
				7.30 ± 0.16^e	7.50^j
3d4p $^1P^o_1$	30 815.70	8.10		8.8 ± 0.4^d	7.35^i
				8.5 ± 0.6^g	8.76^j
				5.5 ± 0.5^h	
3d4p $^1F^o_3$	32 349.98	4.68		5.1 ± 0.3^d	4.46^i
				5.2 ± 0.2^e	5.20^j
				6.8 ± 0.6^h	
4s4p $^3P^o_0$	39 002.20	3.69		3.7 ± 0.2^d	3.36^i
					3.66^j
4s4p $^3P^o_1$	39 115.04	3.69		3.7 ± 0.2^d	3.37^i
					3.67^j
4s4p $^3P^o_2$	39 345.52	3.70		3.8 ± 0.2^d	3.39^i
					3.67^j
4s4p $^1P^o_1$	55 715.36	0.88			0.91^i
3d5s $^3D_1$	57 551.88	3.49			3.44^i
3d5s $^3D_2$	57 614.40	3.50			3.44^i
3d5s $^3D_3$	57 743.92	3.50	3.20 ± 0.20		3.44^i
3d5s $^1D_2$	58 252.09	3.70	3.26 ± 0.20		3.66^j
3d4d $^1F_3$	59 528.42	2.69	2.32 ± 0.15		2.51^i
					2.51^j
3d4d $^3D_1$	59 875.08	2.72	2.23 ± 0.15		2.62^i
3d4d $^3D_2$	59 929.46	2.74	2.32 ± 0.15		2.63^i
					2.58^j
3d4d $^3D_3$	60 001.91	2.76	2.41 ± 0.20		2.65^i
3d4d $^3G_3$	60 267.16	2.50	2.19 ± 0.15	2.5 ± 0.2^d	2.33^i
					2.47^j
3d4d $^3G_4$	60 348.46	2.52		2.4 ± 0.2^d	2.35^i
					2.49^j
3d4d $^1P_1$	60 400.41	2.89	2.44 ± 0.15		2.69^i
					2.63^j
3d4d $^3G_5$	60 457.12	2.54		2.5 ± 0.2^d	2.38^i
					2.51^j
3d4d $^3S_1$	61 071.43	2.82	2.45 ± 0.15		2.77^i
					2.78^j
3d4d $^3F_2$	63 374.63	2.40	2.15 ± 0.10		2.05^i
					2.43^j
3d4d $^3F_3$	63 445.16	2.41			2.05^i
3d4d $^3F_4$	63 528.54	2.43	2.19 ± 0.10		2.07^i
					2.47^j
3d4d $^1D_2$	64 366.68	2.73	2.25 ± 0.15		2.26^i
3d4d $^3P_0$	64 615.77	3.21			2.65^i
3d4d $^3P_1$	64 646.70	3.21			2.65^i
3d4d $^3P_2$	64 705.89	3.19	2.51 ± 0.15		2.65^i
3d4d $^1G_4$	65 236.04	3.17			2.45^i
3d4d $^1S_0$	67 216.56	3.87			2.74^i
$4p^2$ $^1D_2$	74 433.30	5.96	3.80 ± 0.15		6.80^i
$4p^2$ $^3P_0$	76 243.20	1.17			1.28^i
$4p^2$ $^3P_1$	76 360.80	1.17	1.14 ± 0.06		1.28^i
$4p^2$ $^3P_2$	76 589.30	1.18	1.09 ± 0.06		1.30^i
					1.03^j
3d6s $^3D_1$	77 195.19	5.56			5.00^i
3d6s $^3D_2$	77 256.99	5.55			5.00^i
3d6s $^3D_3$	77 387.17	5.54	3.73 ± 0.25		4.98^i
3d6s $^1D_2$	77 833.88	6.61			6.94^i

Notes. [a]Johansson & Litzén (1980).
[b]HFR+CPOL calculation, this work.
[c]TR-LIF measurements, this work.
[d]TR-LIF measurements by Marsden et al. (1988).
[e]TR-LIF measurements by Vogel et al. (1985).
[f]TR-LIF measurements by Arnesen et al. (1976).
[g]Beam–foil spectroscopy by Palenius et al. (1976).
[h]Beam–foil spectroscopy by Buchta et al. (1971).
[i]HFR calculation by Kurucz (2011).
[j]Parametric method calculation by Ruczkowski et al. (2014).

where g_u is the statistical weight of the upper level, g_l the statistical weight of the lower level, λ the wavelength of the transition in Å and A_{ul} the transition probability in s^{-1}.

The transition probability is related to the branching fraction (BF) and the lifetime of the upper level (τ_u). It can be derived using

$$A_{ul} = \frac{BF_{ul}}{\tau_u}. \quad (2)$$

We obtained the lifetimes of the upper levels from our measurements, as discussed in Section 2. The BF is the parameter we measure and it is defined as the transition probability of the line, A_{ul}, divided by the sum of transition probabilities of all lines from the same upper level;

$$BF_{ul} = \frac{A_{ul}}{\sum_i A_{ui}} = \frac{I_{ul}}{\sum_i I_{ui}}. \quad (3)$$

Since all lines emanate from the same upper level, the transition probability is proportional to the line intensity, I_{ul}, which for FTS spectra is proportional to photon flux (Davis, Abrams & Brault 2001). Therefore, we derived BFs from calibrated intensity ratios in our measurements. All lines were identified using the analysis of Johansson & Litzén (1980). The intensities of the observed lines were determined by fitting Gaussian line profiles using GFIT (Engström 1998, 2014).

The uncertainty of the A-value, and thus of the f-value, arises from the uncertainty in the upper level lifetime and the uncertainty of the BF. The latter includes the uncertainty in the intensity calibration procedure and the uncertainty in the measured line intensity, including the self-absorption correction. The uncertainties of the integrated line intensities were determined using GFIT. The relative uncertainties are as low as 0.1 per cent for strong lines and 4 per cent on average. However, for two weak lines the uncertainty is as large as 20 per cent. The uncertainty in the calibration using the tungsten lamp is 2.2 per cent and the uncertainty using the deuterium lamp is 8.6 per cent for the region 425–210 nm and 9.9 per cent for

Table 3. Presentation of experimental log (*gf*) values together with the transition, wavelength, λ, wavenumber, σ, measured branching fraction, $BF_{\rm exp}$, experimental transition probability, $A_{\rm exp}$ and the corresponding rescaled semi-empirical log (*gf*) values of this work. The radiative lifetimes, τ, are TR-LIF measurements from this work.

Upper level[a]		Lower level[a]		$\lambda^a_{\rm exp}$	$\sigma^a_{\rm exp}$	$\sigma^b_{\rm theo}$	$BF_{\rm exp}$	BF unc.	$A_{\rm exp}$	log (*gf*)	log $(gf)_{\rm resc}$
Config.	Energy (cm^{-1})	Config.	Energy (cm^{-1})	(nm)	(cm^{-1})	(cm^{-1})		per cent	(s^{-1})	Exp.	Calc.
3d5s ^{3}D$_3$	57 744	3d4p ^{3}F$^o_3$	27 602	331.673	30 141.50	30 176	6.21E−02	4	1.94E+07	−0.65 ± 0.03	−0.75
τ= 3.20 ± 0.20 ns		3d4p ^{3}F$^o_4$	27 841	334.323	29 902.57	29 944	4.05E−01	3	1.27E+08	0.17 ± 0.03	0.14
		3d4p ^{3}D$^o_2$	28 021	336.347	29 722.58	29 771	5.29E−02	4	1.65E+07	−0.71 ± 0.03	−0.69
		3d4p ^{3}D$^o_3$	28 161	337.938	29 582.76	29 620	3.60E−01	3	1.12E+08	0.13 ± 0.03	0.17
		3d4p ^{3}P$^o_2$	29 824	358.064	27 919.88	27 888	1.20E−01	4	3.75E+07	−0.30 ± 0.03	−0.28
		Residual					3.37E−03				
3d5s ^{1}D$_2$	58 252	3d4p ^{1}D$^o_2$	26 081	310.751	32 179.68	32 040	4.90E−01	2	1.50E+08	0.04 ± 0.03	−0.09
τ= 3.26 ± 0.20 ns		3d4p ^{3}F$^o_2$	27 444	324.493	30 808.34	30 866	1.08E−02	16	3.30E+06	−1.58 ± 0.07	−1.64
		3d4p ^{1}P$^o_1$	30 816	364.376	27 436.43	27 508	1.48E−01	4	4.55E+07	−0.34 ± 0.03	−0.32
		3d4p ^{1}F$^o_3$	32 350	385.960	25 902.13	25 865	3.51E−01	5	1.08E+08	0.08 ± 0.03	0.18
		Residual					2.10E−02				
3d4d ^{1}F$_3$	59 528	3d4p ^{1}D$^o_2$	26 081	298.893	33 447.17	33 296	8.22E−01	0.5	3.54E+08	0.52 ± 0.03	0.47
τ= 2.32 ± 0.15 ns		3d4p ^{3}D$^o_3$	28 161	318.712	31 367.21	31 408	6.54E−03	14	2.82E+06	−1.52 ± 0.06	−1.45
		3d4p ^{1}F$^o_3$	32 350	367.834	27 178.50	27 121	1.72E−01	7	7.40E+07	0.02 ± 0.04	0.20
		Residual					5.10E−03				
3d4d ^{3}D$_1$	59 875	3d4p ^{3}F$^o_2$	27 444	308.254	32 431.14	32 475	1.22E−01	5	5.49E+07	−0.63 ± 0.04	−0.63
τ= 2.23 ± 0.15 ns		3d4p ^{3}D$^o_1$	27 918	312.827	31 957.28	32 026	4.57E−01	3	2.05E+08	−0.04 ± 0.03	−0.11
		3d4p ^{3}D$^o_2$	28 021	313.843	31 853.76	31 913	1.17E−01	5	5.24E+07	−0.63 ± 0.04	−0.65
		3d4p ^{3}P$^o_0$	29 736	331.703	30 138.84	30 134	1.79E−01	4	8.02E+07	−0.40 ± 0.03	−0.37
		3d4p ^{3}P$^o_1$	29 742	331.768	30 132.91	30 123	1.25E−01	5	5.61E+07	−0.56 ± 0.04	−0.50
		Residual					3.75E−02				
3d4d ^{3}D$_2$	59 929	3d4p ^{3}F$^o_3$	27 602	309.249	32 327.05	32 372	1.21E−01	5	5.23E+07	−0.43 ± 0.03	−0.45
τ= 2.32 ± 0.15 ns		3d4p ^{3}D$^o_1$	27 918	312.296	32 011.74	32 081	8.39E−02	5	3.62E+07	−0.58 ± 0.03	−0.63
		3d4p ^{3}D$^o_2$	28 021	313.309	31 908.30	31 968	4.12E−01	3	1.78E+08	0.12 ± 0.03	0.06
		3d4p ^{3}D$^o_3$	28 161	314.688	31 768.28	31 816	6.61E−02	5	2.85E+07	−0.67 ± 0.03	−0.68
		3d4p ^{3}P$^o_1$	29 742	331.170	30 187.30	30 178	2.50E−01	4	1.08E+08	−0.05 ± 0.03	−0.02
		3d4p ^{3}P$^o_2$	29 824	332.069	30 105.53	30 084	6.67E−02	5	2.87E+07	−0.62 ± 0.03	−0.56
		Residual					3.42E−02				
3d4d ^{3}D$_3$	60 002	3d4p ^{3}F$^o_4$	27 841	310.850	32 160.62	32 214	9.39E−02	6	3.90E+07	−0.40 ± 0.04	−0.34
τ= 2.41 ± 0.20 ns		3d4p ^{3}D$^o_2$	28 021	312.599	31 980.37	32 041	4.35E−02	7	1.81E+07	−0.73 ± 0.06	−0.63
		3d4p ^{3}D$^o_3$	28 161	313.972	31 840.77	31 890	5.16E−01	4	2.14E+08	0.35 ± 0.04	0.28
		3d4p ^{3}P$^o_2$	29 824	331.272	30 178.03	30 157	3.47E−01	5	1.44E+08	0.22 ± 0.04	0.24
		Residual					3.51E−02				
3d4d ^{3}G$_3$	60267	3d4p ^{3}F$^o_2$	27 444	304.572	32 823.36	32 822	9.26E−01	1	4.23E+08	0.61 ± 0.03	0.61
τ= 2.19 ± 0.15 ns		3d4p ^{3}F$^o_3$	27 602	306.052	32 664.51	32 664	7.41E−02	8	3.38E+07	−0.48 ± 0.04	−0.47
		Residual					6.20E−03				
3d4d ^{1}P$_1$	60400	3d4p ^{1}D$^o_2$	26 081	291.298	34 319.09	34 206	3.98E−01	7	1.63E+08	−0.21 ± 0.04	−0.33
τ= 2.44 ± 0.15 ns		3d4p ^{1}P$^o_1$	30 816	337.915	29 584.65	29 673	6.02E−01	5	2.47E+08	0.10 ± 0.03	0.14
		Residual					7.27E−02				
3d4d ^{3}S$_1$	61071	3d4p ^{3}P$^o_0$	29 736	319.038	31 335.12	31 336	1.13E−01	7	4.60E+07	−0.68 ± 0.04	−0.70
τ= 2.45 ± 0.15 ns		3d4p ^{3}P$^o_1$	29 742	319.098	31 329.24	31 326	2.84E−01	6	1.16E+08	−0.28 ± 0.04	−0.25
		3d4p ^{3}P$^o_2$	29 824	319.933	31 247.50	31 231	5.73E−01	4	2.34E+08	0.03 ± 0.03	−0.02
		3d4p ^{1}P$^o_1$	30 816	330.421	30 255.76	30 319	3.04E−02	10	1.24E+07	−1.21 ± 0.05	−1.28
		Residual					6.10E−02				
3d4d ^{3}F$_2$	63375	3d4p ^{3}F$^o_2$	27 444	278.230	35 930.81	35 960	3.57E−01	5	1.66E+08	−0.02 ± 0.03	−0.07
τ= 2.15 ± 0.10 ns		3d4p ^{3}F$^o_3$	27 602	279.464	35 772.19	35 802	3.72E−02	9	1.73E+07	−0.99 ± 0.04	−0.95
		3d4p ^{3}D$^o_1$	27 918	281.950	35 456.96	35 511	5.27E−01	3	2.45E+08	0.17 ± 0.02	0.17
		3d4p ^{3}D$^o_2$	28 021	282.776	35 353.30	35 398	7.88E−02	6	3.66E+07	−0.66 ± 0.03	−0.60
		Residual					1.59E−02				
3d4d ^{3}F$_4$	63529	3d4p ^{3}F$^o_4$	27 841	280.130	35 687.12	35 726	3.42E−01	6	1.56E+08	0.22 ± 0.03	0.21
τ= 2.19 ± 0.10 ns		3d4p ^{3}D$^o_3$	28 161	282.663	35 367.30	35 402	6.58E−01	3	3.01E+08	0.51 ± 0.02	0.51
		Residual					8.18E−03				
3d4d ^{1}D$_2$	64367	3d4p ^{1}D$^o_2$	26 081	261.119	38 285.22	38 187	7.25E−01	4	3.22E+08	0.22 ± 0.03	0.11
τ= 2.25 ± 0.15 ns		3d4p ^{3}F$^o_2$	27 444	270.754	36 923.00	37 012	1.69E−02	12	7.51E+06	−1.38 ± 0.06	−1.49
		3d4p ^{3}P$^o_1$	29 742	288.728	34 624.48	34 661	2.27E−02	16	1.01E+07	−1.20 ± 0.07	−1.07

Table 3 – *continued*

Upper level[a] Config.	Energy (cm^{-1})	Lower level[a] Config.	Energy (cm^{-1})	λ^a_{exp} (nm)	σ^a_{exp} (cm^{-1})	σ^b_{theo} (cm^{-1})	BF_{exp}	BF unc. per cent	A_{exp} (s^{-1})	log (gf) Exp.	log (gf)$_{resc}$ Calc.
		$3d4p\ ^1P^o_1$	30 816	297.967	33 550.90	33 654	2.35E−01	8	1.05E+08	−0.16 ± 0.04	−0.02
		Residual					4.94E−02				
$3d4d\ ^3P_2$	64706	$3d4p\ ^3D^o_3$	28 161	273.556	36 544.66	36 597	1.59E−01	8	6.32E+07	−0.45 ± 0.04	−0.46
$\tau = 2.51 \pm 0.15$ ns		$3d4p\ ^3P^o_1$	29 742	285.927	34 963.68	34 960	1.78E−01	6	7.09E+07	−0.36 ± 0.04	−0.40
		$3d4p\ ^3P^o_2$	29 824	286.597	34 881.86	34 865	6.33E−01	3	2.52E+08	0.19 ± 0.03	0.16
		$3d4p\ ^1P^o_1$	30 816	294.984	33 890.19	33 953	3.08E−02	8	1.23E+07	−1.10 ± 0.04	−0.98
		Residual					4.86E−02				
$4p^2\ ^3P_1$	76361	$3d4p\ ^3D^o_2$	28 021	206.804	48 339.50	48 384	3.16E−01	7	2.77E+08	−0.27 ± 0.04	−0.41
$\tau = 1.14 \pm 0.06$ ns		$4s4p\ ^3P^o_0$	39 002	267.597	37 358.69	37 358	2.29E−01	6	2.01E+08	−0.19 ± 0.03	−0.18
		$4s4p\ ^3P^o_1$	39 115	268.407	37 245.53	37 245	1.80E−01	6	1.58E+08	−0.29 ± 0.03	−0.31
		$4s4p\ ^3P^o_2$	39 346	270.079	37 014.70	37 014	2.75E−01	6	2.41E+08	−0.10 ± 0.03	−0.09
		Residual					6.46E−02				
$4p^2\ ^3P_2$	76589	$3d4p\ ^3D^o_2$	28 021	205.831	48 568.03	48 615	5.63E−02	27	5.17E+07	−0.78 ± 0.11	−0.88
$\tau = 1.09 \pm 0.06$ ns		$3d4p\ ^3D^o_3$	28 161	206.426	48 428.15	48 464	2.95E−01	6	2.71E+08	−0.06 ± 0.03	−0.13
		$4s4p\ ^3P^o_1$	39 115	266.771	37 474.35	37 477	1.65E−01	6	1.52E+08	−0.09 ± 0.03	−0.06
		$4s4p\ ^3P^o_2$	39 346	268.422	37 243.72	37 246	4.83E−01	4	4.43E+08	0.38 ± 0.03	0.41
		Residual					1.18E−02				

Note. [a]Energy level, wavelength and wavenumber values are taken from Johansson & Litzén (1980) which are available in NIST data base (Kramida et al. 2015).
[b]Theoretical wavenumber values are from the calculations of this work.

317–158 nm. These calibration lamp uncertainties include the calibration uncertainty and the variation resulting from the repeated measurements made before and after all scandium scans. The uncertainties of the radiative lifetimes are given in Table 2. Finally, we were not able to observe the weakest lines from the investigated level. However, we included their contributions as residuals with derived theoretical *BF*s from our calculations. The residual *BF*s are less than 7 per cent for all levels. The uncertainties in the residuals were estimated to 50 per cent and included in the error budget. The final uncertainties in the oscillator strengths are presented in Table 4 and were derived from the individual contributions using the method described by Sikström et al. (2002).

4 RADIATIVE PARAMETER CALCULATIONS

To calculate branching fractions and the oscillator strengths in Sc II, we used the relativistic Hartree–Fock (HFR) method implemented in the Cowan's suite of atomic structure computer codes (Cowan 1981). It is modified by including a pseudo-potential and a correction to the electric dipole operator which take into account the core-polarization effects giving rise to the HFR+CPOL technique (Quinet et al. 1999).

In this study, the valence–valence correlation was included using the following configuration interaction (CI) expansions: 3d4s + 3d5s + 3d6s + 3d7s + $3d^2$ + 3d4d + 3d5d + 3d6d + 3d7d + 3d5g + 3d6g + 3d7g + $4s^2$+4s5s + 4s6s + 4s7s + 4s4d + 4s5d + 4s6d + 4s7d + 4s5g + 4s6g + 4s7g + $4p^2$ + $4d^2$ + $4f^2$ + 4p4f for the even parity and 3d4p + 3d5p + 3d6p + 3d7p + 3d4f + 3d5f + 3d6f + 3d7f + 3d6h + 3d7h + 4s4p + 4s5p + 4s6p + 4s7p + 4s4f + 4s5f + 4s6f + 4s7f + 4s6h + 4s7h + 4p4d + 4d4f for the odd parity.

Regarding the core-polarization effects, a Sc IV $3p^6$ closed-subshell ionic core was considered where the dipole polarizability, $\alpha_d = 2.129\ a_0^3$, was taken from the relativistic random-phase approximation calculations of Johnson, Kolb & Huang (1983) and a cut-off radius of 1.17 a_0 was estimated as the HFR mean radius of the outermost 3p orbital, $\langle 3p|r|3p\rangle_{HFR}$.

During a least-squares fit procedure, we adjusted some radial integrals to minimize the discrepancies between the Hamiltonian eigenvalues and the experimental energy levels taken from the NIST Atomic Spectra Database (Kramida et al. 2015). The latter are based on the term analysis originally carried out by Russell & Meggers (1927) and later revised by Neufeld (1970) and by Johansson & Litzén (1980). There are 168 levels belonging to the configurations 3d4s, $3d^2$, 3d4p, 4s4p, 3d5s, 3d4d, 3d5p, $4p^2$, 3d4f, 3d6s, 4s5s, 3d5d, 4s4d, 3d5f, 3d5g, 3d7s, 3d6d and 3d6f. The average energies, E_{av}, of the above-mentioned known configurations along with their direct, F^k, exchange, G^k, electrostatic and spin-orbit, ζ, radial parameters were considered in the fit of the energy levels. The *ab initio* and fitted parameter values are reported in Tables 4 and 5 for the even and odd configurations, respectively. The spin-orbit integrals not presented in these tables were fixed to their HFR+CPOL values. The other Slater integrals, including the CI R^k parameters, not reported here, were fixed to 80 per cent of their *ab initio* values to account for missing CI effects (Cowan 1981). The average deviations of the least-squares fits were 157 cm^{-1} for the 93 even-parity experimental levels and 65 cm^{-1} for the 75 odd-parity experimental levels.

5 RESULTS AND DISCUSSION

Table 2 compares our TR-LIF and HFR+CPOL lifetimes with other experimental values from the literature (Buchta et al. 1971; Arnesen et al. 1976; Palenius et al. 1976; Vogel et al. 1985; Marsden et al. 1988), the HFR values calculated by Kurucz (2011) and the lifetimes deduced from the semi-empirical oscillator strengths calculated by Ruczkowski et al. (2014). On average, our HFR+CPOL lifetimes are shorter than the measurements for the odd-parity levels and longer for the even-parity levels. The discrepancies range from a few per cent to about 20 per cent, except for the even-parity levels $4p^2\ ^1D_2$ and $3d6s\ ^3D_3$ where they reach 57 per cent and 49 per cent, respectively. In the former case, this state is strongly mixed (our calculation gives 36 per cent $4p^2\ ^1D_2$ + 36 per cent $4s4d\ ^1D_2$ + 23 per cent $3d6s\ ^1D_2$) and an important decay channel ($4p^2\ ^1D_2 \rightarrow 3d4p\ ^1D^o_2$ $BF = 0.0713$) is

Table 4. Radial parameters adopted in the HFR+CPOL calculations for the even-parity configurations of Sc II. The parameters not listed here have been fixed to their *ab initio* values or to 80 per cent of their HFR+CPOL values for the electrostatic integrals.

Config.	Parameter	*Ab initio* (cm^{-1})	Fitted (cm^{-1})	Ratio	Note[a]
3d4s	E_{av}	1075	1137		
	ζ_{3d}	83	72	0.87	
	G^2(3d4s)	11 351	9883	0.87	
3d5s	E_{av}	57 881	58 144		
	ζ_{3d}	87	79	0.91	
	G^2(3d5s)	2071	1851	0.89	
3d6s	E_{av}	77 397	77 497		
	ζ_{3d}	88	82	0.93	
	G^2(3d6s)	789	631	0.80	F
3d7s	E_{av}	86 487	86 549		
	ζ_{3d}	88	69	0.78	
	G^2(3d7s)	393	314	0.80	F
$3d^2$	E_{av}	11 721	9531		
	F^2(3d3d)	49 657	37 346	0.75	
	F^4(3d3d)	30 556	22 011	0.72	
	α	0	64		
	β	0	−962		
	T	0	3		
	ζ_{3d}	65	59	0.91	
3d4d	E_{av}	62 210	62 852		
	ζ_{3d}	87	79	0.91	
	ζ_{4d}	8	8	1.00	F
	F^2(3d4d)	7539	5977	0.79	
	F^4(3d4d)	3599	2816	0.78	
	G^0(3d4d)	6862	2467	0.36	
	G^2(3d4d)	4352	3238	0.74	
	G^4(3d4d)	2927	2327	0.80	
3d5d	E_{av}	79393	79 170		
	ζ_{3d}	87	86	0.99	
	ζ_{5d}	3	3	1.00	F
	F^2(3d5d)	2896	2158	0.75	
	F^4(3d5d)	1388	1099	0.79	
	G^0(3d5d)	2416	1008	0.42	R
	G^2(3d5d)	1640	684	0.42	R
	G^4(3d5d)	1122	469	0.42	R
3d6d	E_{av}	87550	87 894		
	ζ_{3d}	88	88	1.00	F
	ζ_{6d}	2	2	1.00	F
	F^2(3d6d)	1458	1166	0.80	F
	F^4(3d6d)	705	564	0.80	F
	G^0(3d6d)	1176	941	0.80	F
	G^2(3d6d)	822	658	0.80	F
	G^4(3d6d)	571	454	0.80	F
3d5g	E_{av}	85 492	85 761		
	ζ_{3d}	88	78	0.89	
	ζ_{5g}	0	0	1.00	F
	F^2(3d5g)	465	420	0.90	
	F^4(3d5g)	42	34	0.81	
	G^2(3d5g)	6	5	0.80	F
	G^4(3d5g)	4	3	0.80	F
	G^6(3d5g)	2	2	0.80	F
$4s^2$	E_{av}	16 845	16 876		
4s5s	E_{av}	78 974	79 141		
	G^0(4s5s)	2341	1765	0.75	
4s4d	E_{av}	83 034	82 930		
	ζ_{4d}	9	9	1.00	F
	G^2(4s4d)	6830	5464	0.80	F
$4p^2$	E_{av}	77 789	80 625		
	F^2(4p4p)	28 516	29 802	1.05	
	ζ_{4p}	199	253	1.27	

Note. [a]F and R stand for, respectively, a fixed parameter value and a fixed ratio between these parameters.

Table 5. Radial parameters adopted in the HFR+CPOL calculations for the odd-parity configurations of Sc II. The parameters not listed here have been fixed to their *ab initio* values or to 80 per cent of their HFR+CPOL values for the electrostatic integrals.

Config.	Parameter	*Ab initio* (cm^{-1})	Fitted (cm^{-1})	Ratio	Note[a]
3d4p	E_{av}	28 207	28 996		
	ζ_{3d}	85	91	1.07	
	ζ_{4p}	146	162	1.11	
	F^2(3d4p)	14 647	12 024	0.82	
	G^1(3d4p)	6709	6289	0.94	
	G^3(3d4p)	5361	4338	0.81	
3d5p	E_{av}	66 759	66 915		
	ζ_{3d}	87	73	0.84	
	ζ_{5p}	50	50	1.00	F
	F^2(3d5p)	4168	3375	0.81	
	G^1(3d5p)	1560	1397	0.90	
	G^3(3d5p)	1380	900	0.65	
3d4f	E_{av}	75 021	75 609		
	ζ_{3d}	88	74	0.84	
	ζ_{4f}	0	0	1.00	F
	F^2(3d4f)	2127	1766	0.83	
	F^4(3d4f)	514	367	0.71	
	G^1(3d4f)	420	354	0.84	
	G^3(3d4f)	242	194	0.80	F
	G^5(3d4f)	166	133	0.80	F
3d5f	E_{av}	85 220	85 564		
	ζ_{3d}	88	91	1.03	
	ζ_{5f}	0	0	1.00	F
	F^2(3d5f)	1051	841	0.80	F
	F^4(3d5f)	296	238	0.80	F
	G^1(3d5f)	289	232	0.80	F
	G^3(3d5f)	168	135	0.80	F
	G^5(3d5f)	116	93	0.80	F
3d6f	E_{av}	90 728	91 031		
	ζ_{3d}	88	88	1.00	F
	ζ_{6f}	0	0	1.00	F
	F^2(3d6f)	597	478	0.80	F
	F^4(3d6f)	181	145	0.80	F
	G^1(3d6f)	188	151	0.80	F
	G^3(3d6f)	111	88	0.80	F
	G^5(3d6f)	76	61	0.80	F
4s4p	E_{av}	41 287	43 719		
	ζ_{4p}	197	242	1.23	
	G^1(4s4p)	37 326	27 686	0.74	

Note. [a]F stands for a fixed parameter value.

affected by cancellation (the cancellation factor as defined by Cowan (1981) is less than 5 per cent) that could explain the overestimated lifetime. Concerning 3d6s $^3D_3$ level, no such argument could explain the observed disagreement. The beam–foil measurements of Buchta et al. (1971) can be rejected for the levels 3d4p $^3D^o_3$, $^1P^o_1$ $^1F^o_3$ as previously stated by Marsden et al. (1988) due to blending problems.

The calculations by Kurucz (2011) show roughly the same systematic discrepancy with experiment (lifetimes shorter for the odd parity and longer for the even parity) as our HFR+CPOL calculations. Although the calculation of Kurucz (2011) shows a better agreement than HFR+CPOL for certain 3d4d levels ($^3F_{2,4}$, $^1D_2$ and $^3P_2$), it does not solve the theory–experiment disagreements observed for the levels $4p^2$ $^1D_2$ and 3d6s $^3D_3$. The parametric calculation of Ruczkowski et al. (2014) agrees with our HFR+CPOL model within 10 per cent including all levels. Unfortunately, no lifetime value can be deduced from Ruczkowski et al. (2014) for the levels $4p^2$ $^1D_2$ and 3d6s $^3D_3$. Concerning the level 3d4d $^3G_3$, our

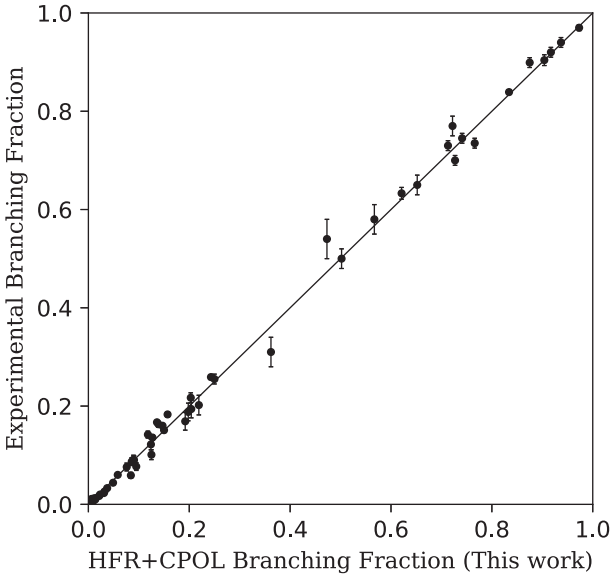

Figure 2. A comparison between the HFR+CPOL branching fractions of this work and the experimental values of Lawler & Dakin (1989). The straight line of equality has been drawn.

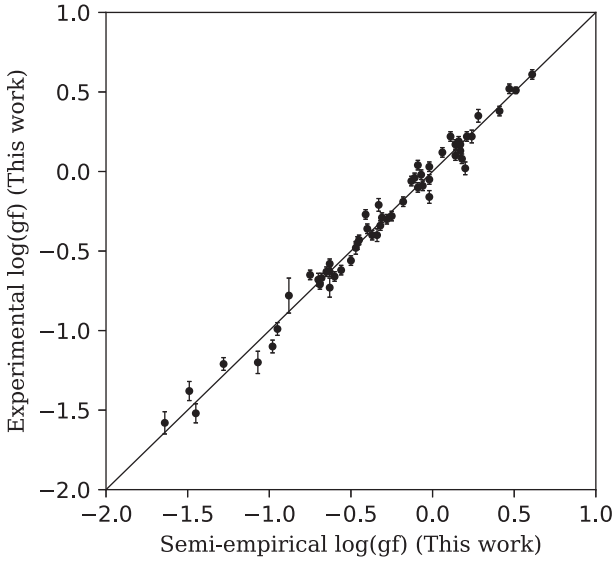

Figure 3. A comparison between the oscillator strengths determined by the combination of the HFR+CPOL branching fractions and the TR-LIF lifetimes of this work and the experimental oscillator strengths derived in this work. The straight line of equality has been drawn.

TR-LIF measurement is slightly lower than the one of Marsden et al. (1988) although the error bars do overlap.

For all 3d4p levels, our HFR+CPOL model and the parametric calculation of Ruczkowski et al. (2014) are closer to the measurement of Marsden et al. (1988). The excellent agreement between Marsden et al. (1988) and Ruczkowski et al. (2014) is not surprising as the latter adjusted the dipole transition integrals to the oscillator strengths determined from the branching fraction measurements of Lawler & Dakin (1989) combined with the lifetime measurements of Marsden et al. (1988). For most of the higher levels, the lifetimes calculated by Kurucz (2011) are closer to our measurements than those of Ruczkowski et al. (2014).

Although there is a systematic discrepancy between the theoretical and experimental lifetimes, we find a better agreement when comparing our calculated *BF*s with the experimental values. For the high excitation lines, measured in this work, the averaged *BF* ratio is 1.02 ± 0.16 with respect to the calculated values. Similarly, Fig. 2 shows the good agreement between *BF*s computed in this study using the HFR+CPOL method and the measurements by Lawler & Dakin (1989). Here, the averaged *BF* ratio is 0.98 ± 0.20. Based on these comparisons, the calculated *BF*s were combined with our TR-LIF lifetimes and those of Marsden et al. (1988) to determine rescaled transition probabilities and oscillator strengths.

In Table 3, we present our experimental $\log(gf)$ values, together with the measured *BF*s, the uncertainties and the corresponding rescaled theoretical oscillator strengths, $\log(gf)_{\rm resc}$. Fig. 3 illustrates the final agreement between our experimental $\log(gf)$ values and the calculated $\log(gf)_{\rm resc}$. Table 6 summarizes our calculated radiative parameters along with the weighted transition probabilities (gA), the weighted oscillator strengths in the log scale ($\log(gf)$), the HFR+CPOL branching fractions (*BF*), and the cancellation factor (*CF*) as defined by Cowan (1981).

Our rescaled theoretical oscillator strengths are compared to the semi-empirical values calculated by Ruczkowski et al. (2014) in Fig. 4. As expected, the scatter increases for the weak lines, i.e. the transitions with $\log(gf) \lesssim -1$, where cancellation effects could be an issue. For instance, the transition 3d4p $^3P^o_2 - 4p^2\ ^3P_2$ labelled in Table 6 $76589(e)2 - 29824(o)2$ has a very low cancellation factor ($CF = 0.001$) that indicates a strong cancellation effect in our HFR+CPOL line strength calculation. Indeed, the rescaled oscillator strength for that transition is $\log(gf)_{\rm resc} = -2.83$ which is three orders of magnitude lower (in the linear scale) than the value predicted by Ruczkowski et al. (2014) ($\log(gf) = -0.02$). On the other hand, a transition for which the cancellation effect in our model is not an issue ($CF > 0.05$) such as 3d4p $^3F^o_3 -$ 3d4d $^3F_4$ $(63529(e)4 - 27602(o)3)$ has an oscillator strength predicted by Ruczkowski et al. (2014) ($\log(gf) = -3.35$) that is two orders of magnitude lower than our rescaled value ($\log(gf)_{\rm resc} = -1.44$). This could indicate a strong cancellation effect in their calculation. Unfortunately, they did not estimate any cancellation factors. For the strongest transitions, i.e. $\log(gf) \gtrsim -1$, the mean scatter drops to about 20 per cent in the linear scale.

In Fig. 5, our semi-empirical values are compared to the calculation of Kurucz (2011) where a similar global correlation is observed. The mean scatter in this case is also found to be ∼20 per cent for transitions with $\log(gf) \gtrsim -1$ and increases for weaker lines. Here again, the cancellation factors are not available in Kurucz's data base (Kurucz 2011). But, for example, our predicted strong line 3d5p $^3F^o_3 -$ 3d6s $^3D_3$ $(77387(e)3 - 66564(o)3)$ with $\log(gf)_{\rm resc} = 0.16$ and $CF = 0.379$ is certainly affected by a strong cancellation effect in the calculation of Kurucz (2011) dramatically lowering its oscillator strength to $\log(gf) = -2.56$.

Based on the differences between different sets of *BF*s discussed above and including the uncertainties of the experimental lifetimes, we estimate the accuracy of the rescaled theoretical *f*-values to be 10 per cent for the strong lines and 15–20 per cent for other lines.

6 CONSEQUENCE ON THE SOLAR ABUNDANCE OF SCANDIUM

Scott et al. (2015) have redetermined the solar abundances of the iron-peak elements employing a 3D model atmosphere that takes into account departures from the local thermodynamic equilibrium. However, the significant discrepancy between the photospheric and

Table 6. Calculated branching fractions (*BFs*), oscillator strengths (log (*gf*)) and transition probabilities (*gA*) along with the corresponding scaled values (log $(gf)_{\rm resc}$, $gA_{\rm resc}$) in Sc II. Only the transitions depopulating the levels for which the lifetime has been measured are listed. The experimental lifetimes (τ_u) used to scale the *f*- and *A*-values are also reported.

Upper level[a]			τ_u (ns)	Lower level[a]			λ[b] (nm)	*BF*	gA (s^{-1})	$gA_{\rm resc}$ (s^{-1})	log (*gf*)	log $(gf)_{\rm resc}$	CF[c]
26 081	(o)	2	7.5[d]	0	(e)	1	383.307	5.91E−03	4.44E+06	3.94E+06	− 2.01	− 2.06	0.468
				68	(e)	2	384.305	1.40E−02	1.05E+07	9.32E+06	− 1.64	− 1.69	0.927
				178	(e)	3	385.938	1.65E−05	1.24E+04	1.10E+04	− 4.56	− 4.61	0.006
				2541	(e)	2	424.682	9.73E−01	7.31E+08	6.49E+08	0.29	0.24	0.975
				4803	(e)	2	469.827	7.55E−04	5.67E+05	5.03E+05	− 2.73	− 2.78	0.260
				4884	(e)	3	471.616	3.77E−05	2.83E+04	2.51E+04	− 4.03	− 4.08	0.047
				10 945	(e)	2	660.460	6.19E−03	4.65E+06	4.13E+06	− 1.53	− 1.57	0.036
				12 102	(e)	1	715.119	6.88E−07	5.17E+02	4.59E+02	− 5.41	− 5.45	0.009
				12 154	(e)	2	717.836	8.89E−06	6.68E+03	5.93E+03	− 4.30	− 4.34	0.008
27 444	(o)	2	6.2[d]	0	(e)	1	364.278	7.27E−01	6.40E+08	5.87E+08	0.11	0.07	0.888
				68	(e)	2	365.180	1.57E−01	1.38E+08	1.26E+08	− 0.56	− 0.60	0.894
				178	(e)	3	366.653	6.61E−03	5.82E+06	5.33E+06	− 1.93	− 1.97	0.927
				2541	(e)	2	401.448	1.27E−02	1.12E+07	1.03E+07	− 1.57	− 1.61	0.837
				4803	(e)	2	441.556	8.94E−02	7.87E+07	7.21E+07	− 0.64	− 0.68	0.971
				4884	(e)	3	443.135	7.01E−03	6.17E+06	5.65E+06	− 1.74	− 1.78	0.466
				10 945	(e)	2	605.924	1.13E−04	9.98E+04	9.15E+04	− 3.26	− 3.30	0.046
				12 102	(e)	1	651.617	2.08E−05	1.83E+04	1.68E+04	− 3.93	− 3.97	0.676
				12 154	(e)	2	653.872	2.60E−06	2.29E+03	2.10E+03	− 4.83	− 4.87	0.053
27 602	(o)	3	6.1[d]	68	(e)	2	363.074	7.66E−01	9.54E+08	8.79E+08	0.28	0.24	0.871
				178	(e)	3	364.531	1.36E−01	1.69E+08	1.56E+08	− 0.47	− 0.51	0.952
				2541	(e)	2	398.906	7.51E−04	9.35E+05	8.62E+05	− 2.65	− 2.69	0.768
				4803	(e)	2	438.481	7.95E−03	9.90E+06	9.12E+06	− 1.54	− 1.58	0.966
				4884	(e)	3	440.039	8.59E−02	1.07E+08	9.86E+07	− 0.51	− 0.54	0.975
				4988	(e)	4	442.067	3.37E−03	4.20E+06	3.87E+06	− 1.91	− 1.95	0.242
				10 945	(e)	2	600.150	4.67E−06	5.82E+03	5.36E+03	− 4.50	− 4.54	0.520
				12 154	(e)	2	647.153	4.47E−05	5.57E+04	5.13E+04	− 3.46	− 3.49	0.612
				14 261	(e)	4	749.355	5.08E−08	6.33E+01	5.83E+01	− 6.28	− 6.31	0.089
27 841	(o)	4	6.1[d]	178	(e)	3	361.383	9.04E−01	1.47E+09	1.33E+09	0.46	0.42	0.949
				4884	(e)	3	435.460	6.12E−03	9.96E+06	9.03E+06	− 1.55	− 1.59	0.976
				4988	(e)	4	437.446	9.04E−02	1.47E+08	1.33E+08	− 0.37	− 0.42	0.976
				14 261	(e)	4	736.173	7.87E−07	1.28E+03	1.16E+03	− 4.99	− 5.03	0.912
27 918	(o)	1	4.7[d]	0	(e)	1	358.092	5.67E−01	3.83E+08	3.62E+08	− 0.13	− 0.16	0.931
				68	(e)	2	358.963	2.03E−01	1.37E+08	1.29E+08	− 0.58	− 0.60	0.950
				2541	(e)	2	393.949	6.08E−06	4.11E+03	3.88E+03	− 5.02	− 5.04	0.001
				4803	(e)	2	432.500	2.19E−01	1.48E+08	1.40E+08	− 0.38	− 0.41	0.961
				10 945	(e)	2	589.000	1.73E−04	1.17E+05	1.11E+05	− 3.21	− 3.24	0.214
				11 736	(e)	0	617.822	4.66E−04	3.15E+05	2.98E+05	− 2.74	− 2.77	0.704
				12 074	(e)	0	630.992	6.22E−03	4.20E+06	3.97E+06	− 1.60	− 1.63	0.611
				12 102	(e)	1	632.085	4.22E−03	2.85E+06	2.69E+06	− 1.77	− 1.79	0.563
				12 154	(e)	2	634.207	2.25E−04	1.52E+05	1.44E+05	− 3.04	− 3.06	0.323
				25 955	(e)	0	5093.945	6.48E−08	4.38E+01	4.14E+01	− 4.72	− 4.79	0.157
28 021	(o)	2	4.7[d]	0	(e)	1	356.770	1.39E−01	1.57E+08	1.48E+08	− 0.52	− 0.55	0.950
				68	(e)	2	357.634	5.02E−01	5.68E+08	5.34E+08	0.04	0.01	0.857
				178	(e)	3	359.047	1.27E−01	1.44E+08	1.35E+08	− 0.55	− 0.58	0.923
				2541	(e)	2	392.348	2.16E−03	2.44E+06	2.29E+06	− 2.25	− 2.28	0.741
				4803	(e)	2	430.571	2.13E−02	2.41E+07	2.26E+07	− 1.17	− 1.20	0.721
				4884	(e)	3	432.073	1.98E−01	2.24E+08	2.10E+08	− 0.20	− 0.23	0.963
				10 945	(e)	2	585.430	8.92E−07	1.01E+03	9.49E+02	− 5.28	− 5.31	0.002
				12 102	(e)	1	627.975	8.83E−03	1.00E+07	9.40E+06	− 1.23	− 1.25	0.651
				12 154	(e)	2	630.070	2.24E−03	2.54E+06	2.39E+06	− 1.82	− 1.85	0.443
28 161	(o)	3	4.7[d]	68	(e)	2	355.853	1.18E−01	1.88E+08	1.76E+08	− 0.45	− 0.48	0.968
				178	(e)	3	357.253	6.52E−01	1.04E+09	9.72E+08	0.30	0.27	0.894
				2541	(e)	2	390.206	2.31E−05	3.69E+04	3.45E+04	− 4.08	− 4.10	0.023
				4803	(e)	2	427.993	3.06E−04	4.88E+05	4.56E+05	− 2.87	− 2.90	0.383
				4884	(e)	3	429.477	1.37E−02	2.18E+07	2.04E+07	− 1.22	− 1.25	0.601
				4988	(e)	4	431.408	2.04E−01	3.26E+08	3.05E+08	− 0.04	− 0.07	0.963
				10 945	(e)	2	580.673	1.57E−04	2.50E+05	2.34E+05	− 2.90	− 2.93	0.555
				12 154	(e)	2	624.564	1.10E−02	1.76E+07	1.64E+07	− 0.99	− 1.02	0.638
				14 261	(e)	4	719.234	3.06E−05	4.88E+04	4.56E+04	− 3.42	− 3.45	0.419
29 736	(o)	0	7.7[d]	0	(e)	1	336.193	8.75E−01	1.38E+08	1.14E+08	− 0.63	− 0.72	0.519
				12 102	(e)	1	566.904	1.25E−01	1.98E+07	1.63E+07	− 1.02	− 1.10	0.885

Table 6 – *continued*

Upper level[a]			τ_u (ns)	Lower level[a]			λ^b (nm)	*BF*	gA (s^{-1})	gA_{resc} (s^{-1})	log (gf)	log $(gf)_{resc}$	CF[c]
29 742	(o)	1	7.6[d]	0	(e)	1	336.127	2.43E−01	1.14E+08	9.57E+07	− 0.72	− 0.79	0.538
				68	(e)	2	336.894	6.21E−01	2.92E+08	2.45E+08	− 0.30	− 0.38	0.485
				2541	(e)	2	367.526	4.00E−03	1.88E+06	1.58E+06	− 2.42	− 2.49	0.070
				4803	(e)	2	400.860	2.21E−04	1.04E+05	8.73E+04	− 3.60	− 3.68	0.479
				10 945	(e)	2	531.835	8.60E−03	4.04E+06	3.39E+06	− 1.77	− 1.84	0.723
				11 736	(e)	0	555.222	5.30E−03	2.49E+06	2.09E+06	− 1.94	− 2.01	0.771
				12 074	(e)	0	565.836	3.72E−02	1.75E+07	1.47E+07	− 1.08	− 1.15	0.736
				12 102	(e)	1	566.715	3.19E−02	1.50E+07	1.26E+07	− 1.15	− 1.22	0.881
				12 154	(e)	2	568.420	4.89E−02	2.30E+07	1.93E+07	− 0.96	− 1.03	0.813
				25 955	(e)	0	2639.920	7.02E−06	3.30E+03	2.77E+03	− 3.46	− 3.54	0.175
29 824	(o)	2	7.4[d]	0	(e)	1	335.205	1.05E−02	8.36E+06	7.12E+06	− 1.85	− 1.92	0.529
				68	(e)	2	335.968	1.47E−01	1.17E+08	9.96E+07	− 0.71	− 0.77	0.537
				178	(e)	3	337.215	7.13E−01	5.66E+08	4.82E+08	− 0.02	− 0.09	0.506
				2541	(e)	2	366.425	2.42E−03	1.92E+06	1.63E+06	− 2.42	− 2.48	0.731
				4803	(e)	2	399.550	3.24E−05	2.57E+04	2.19E+04	− 4.21	− 4.28	0.865
				4884	(e)	3	400.843	1.69E−04	1.34E+05	1.14E+05	− 3.49	− 3.56	0.912
				10 945	(e)	2	529.531	4.02E−04	3.19E+05	2.72E+05	− 2.88	− 2.94	0.210
				12 102	(e)	1	564.100	3.08E−02	2.44E+07	2.08E+07	− 0.94	− 1.00	0.825
				12 154	(e)	2	565.790	9.49E−02	7.53E+07	6.41E+07	− 0.45	− 0.51	0.879
30816	(o)	1	8.8[d]	0	(e)	1	324.416	7.98E−04	2.95E+05	2.72E+05	− 3.33	− 3.37	0.025
				68	(e)	2	325.131	2.31E−02	8.56E+06	7.89E+06	− 1.87	− 1.90	0.259
				2541	(e)	2	353.571	4.73E−01	1.75E+08	1.61E+08	− 0.49	− 0.52	0.193
				4803	(e)	2	384.317	2.68E−04	9.91E+04	9.14E+04	− 3.66	− 3.69	0.065
				10 945	(e)	2	503.102	3.62E−01	1.34E+08	1.24E+08	− 0.29	− 0.33	0.723
				11 736	(e)	0	523.981	1.24E−01	4.60E+07	4.24E+07	− 0.72	− 0.76	0.685
				12 074	(e)	0	533.424	8.14E−03	3.01E+06	2.77E+06	− 1.89	− 1.93	0.773
				12 102	(e)	1	534.205	7.73E−04	2.86E+05	2.64E+05	− 2.91	− 2.95	0.422
				12 154	(e)	2	535.720	6.06E−03	2.24E+06	2.06E+06	− 2.01	− 2.05	0.758
				25 955	(e)	0	2056.840	8.71E−04	3.22E+05	2.97E+05	− 1.67	− 1.73	0.214
32 350	(o)	3	5.1[d]	68	(e)	2	309.678	5.40E−04	8.08E+05	7.41E+05	− 2.94	− 2.97	0.182
				178	(e)	3	310.737	5.99E−04	8.97E+05	8.22E+05	− 2.89	− 2.92	0.835
				2541	(e)	2	335.372	7.22E−01	1.08E+09	9.90E+08	0.26	0.22	0.640
				4803	(e)	2	362.911	2.65E−04	3.96E+05	3.63E+05	− 3.11	− 3.14	0.722
				4884	(e)	3	363.977	1.13E−05	1.69E+04	1.55E+04	− 4.47	− 4.51	0.411
				4988	(e)	4	365.364	9.09E−05	1.36E+05	1.25E+05	− 3.57	− 3.60	0.222
				10 945	(e)	2	467.041	8.42E−02	1.26E+08	1.16E+08	− 0.39	− 0.42	0.625
				12 154	(e)	2	495.020	4.18E−04	6.25E+05	5.73E+05	− 2.64	− 2.68	0.621
				14 261	(e)	4	552.679	1.92E−01	2.88E+08	2.64E+08	0.12	0.08	0.917
39 002	(o)	0	3.7[d]	0	(e)	1	256.319	9.94E−01	2.70E+08	2.69E+08	− 0.58	− 0.58	0.958
				12 102	(e)	1	371.632	5.85E−03	1.59E+06	1.58E+06	− 2.48	− 2.48	0.139
39 115	(o)	1	3.7[d]	0	(e)	1	255.580	2.50E−01	2.04E+08	2.03E+08	− 0.70	− 0.70	0.958
				68	(e)	2	256.023	7.41E−01	6.04E+08	6.01E+08	− 0.23	− 0.23	0.955
				2541	(e)	2	273.337	4.16E−04	3.39E+05	3.37E+05	− 3.42	− 3.42	0.244
				4803	(e)	2	291.357	4.23E−07	3.45E+02	3.43E+02	− 6.36	− 6.36	0.362
				10 945	(e)	2	354.880	2.80E−05	2.28E+04	2.27E+04	− 4.37	− 4.37	0.095
				11 736	(e)	0	365.144	5.13E−07	4.18E+02	4.16E+02	− 6.08	− 6.08	0.001
				12 074	(e)	0	369.704	1.94E−03	1.58E+06	1.57E+06	− 2.49	− 2.49	0.137
				12 102	(e)	1	370.079	1.44E−03	1.17E+06	1.16E+06	− 2.62	− 2.62	0.137
				12 154	(e)	2	370.806	2.36E−03	1.92E+06	1.91E+06	− 2.40	− 2.40	0.136
				25 955	(e)	0	759.679	5.27E−07	4.29E+02	4.27E+02	− 5.43	− 5.43	0.074
39 346	(o)	2	3.8[d]	0	(e)	1	254.082	1.02E−02	1.38E+07	1.34E+07	− 1.88	− 1.89	0.957
				68	(e)	2	254.520	1.50E−01	2.04E+08	1.98E+08	− 0.70	− 0.72	0.957
				178	(e)	3	255.235	8.34E−01	1.13E+09	1.10E+09	0.04	0.03	0.956
				2541	(e)	2	271.625	2.29E−04	3.10E+05	3.01E+05	− 3.47	− 3.48	0.829
				4803	(e)	2	289.412	1.49E−07	2.02E+02	1.96E+02	− 6.60	− 6.61	0.745
				4884	(e)	3	290.090	4.46E−07	6.05E+02	5.87E+02	− 6.12	− 6.13	0.917
				10 945	(e)	2	352.000	2.32E−05	3.14E+04	3.05E+04	− 4.23	− 4.25	0.097
				12 102	(e)	1	366.949	1.36E−03	1.85E+06	1.80E+06	− 2.43	− 2.44	0.129
				12 154	(e)	2	367.663	4.12E−03	5.58E+06	5.42E+06	− 1.95	− 1.96	0.132
57 744	(e)	3	3.20[e]	26 081	(o)	2	315.739	5.95E−06	1.19E+04	1.30E+04	− 4.75	− 4.71	0.004
				27 444	(o)	2	329.936	1.75E−03	3.49E+06	3.82E+06	− 2.25	− 2.21	0.660
				27 602	(o)	3	331.673	4.87E−02	9.74E+07	1.07E+08	− 0.80	− 0.75	0.694
				27 841	(o)	4	334.323	3.77E−01	7.53E+08	8.24E+08	0.10	0.14	0.668

Table 6 – *continued*

Upper level[a]			τ_u (ns)	Lower level[a]			λ^b (nm)	*BF*	gA (s^{-1})	gA_{resc} (s^{-1})	log (gf)	log $(gf)_{resc}$	CF[c]
				28 021	(o)	2	336.347	5.55E−02	1.11E+08	1.21E+08	− 0.73	− 0.69	0.851
				28 161	(o)	3	337.938	3.93E−01	7.86E+08	8.60E+08	0.13	0.17	0.834
				29 824	(o)	2	358.064	1.24E−01	2.47E+08	2.70E+08	− 0.32	− 0.28	0.458
				32 350	(o)	3	393.683	8.95E−05	1.79E+05	1.96E+05	− 3.38	− 3.34	0.357
				39 346	(o)	2	543.375	5.65E−04	1.13E+06	1.24E+06	− 2.30	− 2.26	0.027
58 252	(e)	2	3.26[e]	26 081	(o)	2	310.751	3.70E−01	4.99E+08	5.67E+08	− 0.14	− 0.09	0.549
				27 444	(o)	2	324.493	9.48E−03	1.28E+07	1.45E+07	− 1.70	− 1.64	0.583
				27 602	(o)	3	326.174	7.63E−03	1.03E+07	1.17E+07	− 1.79	− 1.73	0.542
				27 918	(o)	1	329.565	3.92E−04	5.29E+05	6.01E+05	− 3.07	− 3.01	0.062
				28 021	(o)	2	330.693	1.11E−02	1.50E+07	1.70E+07	− 1.61	− 1.55	0.754
				28 161	(o)	3	332.231	7.48E−04	1.01E+06	1.15E+06	− 2.78	− 2.72	0.136
				29 742	(o)	1	350.655	4.07E−04	5.50E+05	6.25E+05	− 2.99	− 2.94	0.016
				29 824	(o)	2	351.663	1.91E−03	2.58E+06	2.93E+06	− 2.32	− 2.26	0.439
				30 816	(o)	1	364.376	1.56E−01	2.10E+08	2.39E+08	− 0.38	− 0.32	0.524
				32 350	(o)	3	385.960	4.43E−01	5.98E+08	6.79E+08	0.13	0.18	0.811
				39 115	(o)	1	522.401	6.04E−07	8.16E+02	9.27E+02	− 5.48	− 5.42	0.001
				39 346	(o)	2	528.770	5.48E−06	7.40E+03	8.41E+03	− 4.51	− 4.45	0.032
				55 715	(o)	1	3941.008	1.07E−04	1.45E+05	1.65E+05	− 1.48	− 1.42	0.272
59 528	(e)	3	2.32[e]	26 081	(o)	2	298.893	7.30E−01	1.90E+09	2.20E+09	0.41	0.47	0.813
				27 444	(o)	2	311.585	5.11E−04	1.33E+06	1.54E+06	− 2.71	− 2.65	0.017
				27 602	(o)	3	313.134	1.28E−03	3.34E+06	3.87E+06	− 2.31	− 2.24	0.483
				27 841	(o)	4	315.495	1.30E−03	3.38E+06	3.92E+06	− 2.30	− 2.23	0.444
				28 021	(o)	2	317.297	8.37E−05	2.18E+05	2.53E+05	− 3.48	− 3.42	0.013
				28 161	(o)	3	318.712	7.76E−03	2.02E+07	2.34E+07	− 1.51	− 1.45	0.493
				29 824	(o)	2	336.553	2.29E−03	5.97E+06	6.92E+06	− 1.99	− 1.93	0.229
				32 350	(o)	3	367.834	2.57E−01	6.69E+08	7.75E+08	0.14	0.20	0.867
				39 346	(o)	2	495.331	1.85E−04	4.81E+05	5.57E+05	− 2.75	− 2.69	0.621
59 875	(e)	1	2.23[e]	26 081	(o)	2	295.826	1.55E−02	1.71E+07	2.09E+07	− 1.64	− 1.56	0.658
				27 444	(o)	2	308.254	1.22E−01	1.34E+08	1.64E+08	− 0.72	− 0.63	0.631
				27 918	(o)	1	312.827	3.93E−01	4.33E+08	5.29E+08	− 0.20	− 0.11	0.597
				28 021	(o)	2	313.843	1.12E−01	1.23E+08	1.50E+08	− 0.74	− 0.65	0.481
				29 736	(o)	0	331.703	1.92E−01	2.11E+08	2.58E+08	− 0.46	− 0.37	0.899
				29 742	(o)	1	331.768	1.42E−01	1.57E+08	1.92E+08	− 0.59	− 0.50	0.750
				29 824	(o)	2	332.670	7.03E−03	7.74E+06	9.45E+06	− 1.89	− 1.80	0.463
				30 816	(o)	1	344.024	9.17E−04	1.01E+06	1.23E+06	− 2.75	− 2.66	0.021
				39 002	(o)	0	478.957	9.08E−03	1.00E+07	1.22E+07	− 1.46	− 1.38	0.769
				39 115	(o)	1	481.560	6.81E−03	7.50E+06	9.16E+06	− 1.58	− 1.50	0.766
				39 346	(o)	2	486.967	3.60E−04	3.97E+05	4.85E+05	− 2.85	− 2.76	0.542
				55 715	(o)	1	2403.352	2.00E−05	2.20E+04	2.69E+04	− 2.72	− 2.63	0.500
59 929	(e)	2	2.32[e]	26 081	(o)	2	295.351	5.27E−05	9.68E+04	1.14E+05	− 3.89	− 3.83	0.011
				27 444	(o)	2	307.738	9.53E−03	1.75E+07	2.05E+07	− 1.61	− 1.53	0.294
				27 602	(o)	3	309.249	1.16E−01	2.13E+08	2.50E+08	− 0.52	− 0.45	0.667
				27 918	(o)	1	312.296	7.46E−02	1.37E+08	1.61E+08	− 0.70	− 0.63	0.512
				28 021	(o)	2	313.309	3.62E−01	6.64E+08	7.79E+08	− 0.01	0.06	0.578
				28 161	(o)	3	314.688	6.48E−02	1.19E+08	1.40E+08	− 0.76	− 0.68	0.420
				29 742	(o)	1	331.170	2.71E−01	4.97E+08	5.83E+08	− 0.09	− 0.02	0.907
				29 824	(o)	2	332.069	7.73E−02	1.42E+08	1.67E+08	− 0.63	− 0.56	0.690
				30 816	(o)	1	343.382	3.84E−03	7.06E+06	8.29E+06	− 1.91	− 1.83	0.362
				32 350	(o)	3	362.485	4.89E−06	8.98E+03	1.05E+04	− 4.75	− 4.68	0.022
				39 115	(o)	1	480.302	1.24E−02	2.28E+07	2.68E+07	− 1.10	− 1.03	0.783
				39 346	(o)	2	485.680	3.79E−03	6.96E+06	8.17E+06	− 1.61	− 1.54	0.716
				55 715	(o)	1	2372.344	1.32E−09	2.42E+00	2.84E+00	− 6.69	− 6.62	0.003
60 002	(e)	3	2.41[e]	26 081	(o)	2	294.720	5.91E−03	1.50E+07	1.72E+07	− 1.71	− 1.65	0.241
				27 444	(o)	2	307.053	9.57E−04	2.43E+06	2.78E+06	− 2.47	− 2.41	0.144
				27 602	(o)	3	308.558	3.10E−03	7.86E+06	9.00E+06	− 1.95	− 1.89	0.088
				27 841	(o)	4	310.850	1.09E−01	2.76E+08	3.16E+08	− 0.40	− 0.34	0.677
				28 021	(o)	2	312.599	5.52E−02	1.40E+08	1.60E+08	− 0.69	− 0.63	0.476
				28 161	(o)	3	313.972	4.41E−01	1.12E+09	1.28E+09	0.22	0.28	0.569
				29 824	(o)	2	331.272	3.63E−01	9.22E+08	1.06E+09	0.18	0.24	0.916
				32 350	(o)	3	361.535	5.75E−03	1.46E+07	1.67E+07	− 1.54	− 1.48	0.807
				39 346	(o)	2	483.977	1.58E−02	4.00E+07	4.58E+07	− 0.85	− 0.79	0.794
60 267	(e)	3	2.19[e]	26 081	(o)	2	292.433	2.06E−03	5.78E+06	6.59E+06	− 2.13	− 2.07	0.062
				27 444	(o)	2	304.572	9.17E−01	2.57E+09	2.93E+09	0.55	0.61	0.862
				27 602	(o)	3	306.052	7.60E−02	2.13E+08	2.43E+08	− 0.52	− 0.47	0.784

Table 6 – *continued*

Upper level[a]			τ_u (ns)	Lower level[a]			λ^b (nm)	*BF*	gA (s^{-1})	gA_{resc} (s^{-1})	log (gf)	log $(gf)_{resc}$	CF[c]
				27 841	(o)	4	308.307	7.21E−04	2.02E+06	2.30E+06	− 2.54	− 2.48	0.321
				28 021	(o)	2	310.027	1.66E−03	4.65E+06	5.30E+06	− 2.17	− 2.12	0.469
				28 161	(o)	3	311.378	9.67E−04	2.71E+06	3.09E+06	− 2.40	− 2.35	0.618
				29 824	(o)	2	328.386	2.14E−04	5.99E+05	6.83E+05	− 3.01	− 2.96	0.858
				32 350	(o)	3	358.100	1.44E−03	4.03E+06	4.60E+06	− 2.11	− 2.05	0.870
				39 346	(o)	2	477.840	6.67E−06	1.87E+04	2.13E+04	− 4.19	− 4.14	0.781
60 348	(e)	4	2.4[d]	27 602	(o)	3	305.292	9.37E−01	3.35E+09	3.52E+09	0.67	0.69	0.863
				27 841	(o)	4	307.536	5.82E−02	2.08E+08	2.18E+08	− 0.53	− 0.51	0.781
				28 161	(o)	3	310.592	4.25E−03	1.52E+07	1.60E+07	− 1.66	− 1.64	0.846
				32 350	(o)	3	357.060	7.98E−05	2.85E+05	2.99E+05	− 3.26	− 3.24	0.295
60 400	(e)	1	2.44[e]	26 081	(o)	2	291.298	2.97E−01	3.08E+08	3.65E+08	− 0.41	− 0.33	0.746
				27 444	(o)	2	303.340	1.18E−02	1.23E+07	1.46E+07	− 1.77	− 1.70	0.731
				27 918	(o)	1	307.767	2.40E−03	2.49E+06	2.95E+06	− 2.45	− 2.38	0.076
				28 021	(o)	2	308.751	4.66E−03	4.84E+06	5.73E+06	− 2.16	− 2.09	0.499
				29 736	(o)	0	326.020	1.01E−02	1.05E+07	1.24E+07	− 1.78	− 1.70	0.891
				29 742	(o)	1	326.082	1.70E−02	1.76E+07	2.08E+07	− 1.55	− 1.48	0.255
				29 824	(o)	2	326.955	3.85E−03	4.00E+06	4.74E+06	− 2.19	− 2.12	0.314
				30 816	(o)	1	337.915	6.51E−01	6.76E+08	8.01E+08	0.06	0.14	0.880
				39 002	(o)	0	467.198	5.28E−04	5.48E+05	6.49E+05	− 2.75	− 2.67	0.735
				39 115	(o)	1	469.675	1.63E−05	1.69E+04	2.00E+04	− 4.26	− 4.18	0.014
				39 346	(o)	2	474.816	3.58E−04	3.72E+05	4.41E+05	− 2.90	− 2.83	0.590
				55 715	(o)	1	2133.866	1.43E−03	1.48E+06	1.75E+06	− 1.00	− 0.92	0.554
60 457	(e)	5	2.5[d]	27 841	(o)	4	306.511	1.00E+00	4.33E+09	4.40E+09	0.79	0.79	0.865
61 071	(e)	1	2.45[e]	26 081	(o)	2	285.711	6.87E−04	7.30E+05	8.41E+05	− 3.05	− 2.99	0.084
				27 444	(o)	2	297.287	1.30E−05	1.38E+04	1.59E+04	− 4.74	− 4.68	0.061
				27 918	(o)	1	301.538	8.24E−05	8.76E+04	1.01E+05	− 3.93	− 3.86	0.091
				28 021	(o)	2	302.483	6.95E−05	7.39E+04	8.51E+04	− 4.00	− 3.93	0.056
				29 736	(o)	0	319.038	1.06E−01	1.13E+08	1.30E+08	− 0.76	− 0.70	0.841
				29 742	(o)	1	319.098	3.00E−01	3.19E+08	3.68E+08	− 0.31	− 0.25	0.802
				29 824	(o)	2	319.933	5.06E−01	5.38E+08	6.20E+08	− 0.08	− 0.02	0.837
				30 816	(o)	1	330.421	2.64E−02	2.81E+07	3.24E+07	− 1.34	− 1.28	0.895
				39 002	(o)	0	452.993	6.99E−03	7.43E+06	8.56E+06	− 1.64	− 1.58	0.718
				39 115	(o)	1	455.321	2.08E−02	2.21E+07	2.55E+07	− 1.17	− 1.10	0.750
				39 346	(o)	2	460.151	3.23E−02	3.43E+07	3.95E+07	− 0.96	− 0.90	0.742
				55 715	(o)	1	1866.531	1.98E−05	2.10E+04	2.42E+04	− 2.96	− 2.90	0.528
63 375	(e)	2	2.15[e]	26 081	(o)	2	268.065	1.38E−02	2.88E+07	3.21E+07	− 1.51	− 1.46	0.561
				27 444	(o)	2	278.230	3.17E−01	6.61E+08	7.37E+08	− 0.12	− 0.07	0.673
				27 602	(o)	3	279.464	4.12E−02	8.59E+07	9.58E+07	− 1.00	− 0.95	0.701
				27 918	(o)	1	281.950	5.37E−01	1.12E+09	1.25E+09	0.12	0.17	0.685
				28 021	(o)	2	282.776	8.92E−02	1.86E+08	2.07E+08	− 0.65	− 0.60	0.516
				28 161	(o)	3	283.899	1.87E−03	3.91E+06	4.36E+06	− 2.33	− 2.28	0.263
				29 742	(o)	1	297.245	3.20E−05	6.68E+04	7.45E+04	− 4.05	− 4.01	0.023
				29 824	(o)	2	297.969	2.25E−05	4.70E+04	5.24E+04	− 4.20	− 4.16	0.075
				30 816	(o)	1	307.046	2.30E−06	4.79E+03	5.34E+03	− 5.17	− 5.12	0.000
				32 350	(o)	3	322.231	1.81E−04	3.77E+05	4.20E+05	− 3.23	− 3.18	0.221
				39 115	(o)	1	412.092	1.83E−06	3.81E+03	4.25E+03	− 5.01	− 4.97	0.218
				39 346	(o)	2	416.045	3.25E−07	6.78E+02	7.56E+02	− 5.76	− 5.71	0.068
				55 715	(o)	1	1305.250	5.75E−06	1.20E+04	1.34E+04	− 3.51	− 3.47	0.207
63 529	(e)	4	2.19[e]	27 602	(o)	3	278.267	7.54E−03	2.79E+07	3.10E+07	− 1.49	− 1.44	0.119
				27 841	(o)	4	280.130	3.33E−01	1.23E+09	1.37E+09	0.16	0.21	0.704
				28 161	(o)	3	282.663	6.60E−01	2.44E+09	2.71E+09	0.47	0.51	0.697
				32 350	(o)	3	320.641	3.38E−05	1.25E+05	1.39E+05	− 3.71	− 3.67	0.014
64 367	(e)	2	2.25[e]	26 081	(o)	2	261.119	5.63E−01	1.03E+09	1.25E+09	0.03	0.11	0.410
				27 444	(o)	2	270.754	1.32E−02	2.41E+07	2.93E+07	− 1.58	− 1.49	0.444
				27 602	(o)	3	271.923	5.47E−04	1.00E+06	1.21E+06	− 2.96	− 2.87	0.510
				27 918	(o)	1	274.276	3.89E−04	7.11E+05	8.64E+05	− 3.10	− 3.01	0.023
				28 021	(o)	2	275.057	4.30E−04	7.87E+05	9.56E+05	− 3.05	− 2.96	0.021
				28 161	(o)	3	276.120	8.53E−03	1.56E+07	1.90E+07	− 1.75	− 1.66	0.258
				29 742	(o)	1	288.728	3.03E−02	5.55E+07	6.74E+07	− 1.16	− 1.07	0.503
				29 824	(o)	2	289.412	1.85E−02	3.38E+07	4.11E+07	− 1.37	− 1.29	0.305
				30 816	(o)	1	297.967	3.20E−01	5.85E+08	7.11E+08	− 0.11	− 0.02	0.567
				32 350	(o)	3	312.247	4.32E−02	7.90E+07	9.60E+07	− 0.94	− 0.85	0.207
				39 115	(o)	1	395.902	3.40E−05	6.22E+04	7.56E+04	− 3.84	− 3.75	0.017

Table 6 – *continued*

Upper level[a]			τ_u (ns)	Lower level[a]			λ^b (nm)	*BF*	gA (s^{-1})	gA_{resc} (s^{-1})	log (gf)	log (gf)$_{resc}$	CF[c]
				39 346	(o)	2	399.549	9.57E−05	1.75E+05	2.13E+05	− 3.38	− 3.29	0.021
				55 715	(o)	1	1155.577	1.90E−03	3.48E+06	4.23E+06	− 1.16	− 1.07	0.207
64 706	(e)	2	2.51[e]	26 081	(o)	2	258.825	2.19E−02	3.43E+07	4.36E+07	− 1.46	− 1.36	0.199
				27 444	(o)	2	268.289	8.23E−04	1.29E+06	1.64E+06	− 2.86	− 2.75	0.238
				27 602	(o)	3	269.437	6.38E−04	9.99E+05	1.27E+06	− 2.97	− 2.86	0.208
				27 918	(o)	1	271.746	8.55E−04	1.34E+06	1.70E+06	− 2.83	− 2.72	0.055
				28 021	(o)	2	272.513	2.21E−02	3.46E+07	4.40E+07	− 1.42	− 1.31	0.154
				28 161	(o)	3	273.556	1.56E−01	2.44E+08	3.10E+08	− 0.56	− 0.46	0.252
				29 742	(o)	1	285.927	1.63E−01	2.56E+08	3.26E+08	− 0.50	− 0.40	0.424
				29 824	(o)	2	286.597	5.87E−01	9.20E+08	1.17E+09	0.06	0.16	0.545
				30 816	(o)	1	294.984	4.05E−02	6.35E+07	8.07E+07	− 1.08	− 0.98	0.562
				32 350	(o)	3	308.973	3.45E−03	5.40E+06	6.87E+06	− 2.11	− 2.01	0.222
				39 115	(o)	1	390.654	7.53E−04	1.18E+06	1.50E+06	− 2.57	− 2.46	0.021
				39 346	(o)	2	394.204	2.45E−03	3.84E+06	4.88E+06	− 2.05	− 1.94	0.024
				55 715	(o)	1	1111.977	1.19E−04	1.87E+05	2.38E+05	− 2.46	− 2.36	0.198
74 433	(e)	2	3.80[e]	26 081	(o)	2	206.751	7.13E−02	5.98E+07	9.38E+07	− 1.42	− 1.22	0.047
				27 444	(o)	2	212.746	1.00E−03	8.40E+05	1.32E+06	− 3.25	− 3.05	0.054
				27 602	(o)	3	213.467	5.58E−05	4.68E+04	7.34E+04	− 4.51	− 4.30	0.083
				27 918	(o)	1	214.914	8.51E−07	7.14E+02	1.12E+03	− 6.32	− 6.11	0.000
				28 021	(o)	2	215.394	2.11E−04	1.77E+05	2.78E+05	− 3.92	− 3.71	0.024
				28 161	(o)	3	216.045	1.07E−02	8.94E+06	1.40E+07	− 2.21	− 2.01	0.455
				29 742	(o)	1	223.689	5.46E−04	4.58E+05	7.19E+05	− 3.47	− 3.27	0.005
				29 824	(o)	2	224.099	2.39E−05	2.00E+04	3.14E+04	− 4.83	− 4.63	0.001
				30 816	(o)	1	229.195	4.05E−03	3.40E+06	5.34E+06	− 2.58	− 2.38	0.002
				32 350	(o)	3	237.551	8.23E−01	6.90E+08	1.08E+09	− 0.24	− 0.04	0.251
				39 115	(o)	1	283.056	2.83E−03	2.37E+06	3.72E+06	− 2.56	− 2.35	0.244
				39 346	(o)	2	284.916	1.05E−02	8.83E+06	1.39E+07	− 1.98	− 1.77	0.660
				55 715	(o)	1	534.098	4.13E−04	3.46E+05	5.43E+05	− 2.85	− 2.63	0.000
				66 048	(o)	2	1192.292	3.94E−02	3.30E+07	5.18E+07	− 0.20	0.04	0.693
				66 390	(o)	1	1242.891	4.01E−05	3.36E+04	5.27E+04	− 3.17	− 2.91	0.227
				66 493	(o)	2	1259.000	6.15E−05	5.16E+04	8.10E+04	− 2.97	− 2.72	0.112
				66 460	(o)	2	1253.786	1.25E−03	1.05E+06	1.65E+06	− 1.66	− 1.41	0.403
				66 564	(o)	3	1270.370	2.48E−04	2.08E+05	3.26E+05	− 2.36	− 2.10	0.374
				66 584	(o)	3	1273.628	8.54E−05	7.16E+04	1.12E+05	− 2.82	− 2.56	0.390
				67 298	(o)	1	1401.037	5.56E−05	4.66E+04	7.31E+04	− 2.93	− 2.67	0.085
				67 396	(o)	2	1420.650	7.89E−07	6.62E+02	1.04E+03	− 4.76	− 4.50	0.003
				67 744	(o)	3	1494.454	2.93E−02	2.46E+07	3.86E+07	− 0.15	0.11	0.695
				68 498	(o)	1	1684.392	5.06E−03	4.24E+06	6.65E+06	− 0.82	− 0.55	0.165
76 361	(e)	1	1.14[e]	26 081	(o)	2	198.888	2.24E−04	5.75E+05	5.91E+05	− 3.47	− 3.46	0.126
				27 444	(o)	2	204.362	3.68E−04	9.44E+05	9.70E+05	− 3.23	− 3.22	0.387
				27 918	(o)	1	206.362	7.57E−02	1.94E+08	1.99E+08	− 0.91	− 0.90	0.507
				28 021	(o)	2	206.804	2.30E−01	5.88E+08	6.04E+08	− 0.42	− 0.41	0.527
				29 736	(o)	0	214.412	9.25E−05	2.37E+05	2.43E+05	− 3.79	− 3.77	0.000
				29 742	(o)	1	214.439	2.71E−04	6.93E+05	7.12E+05	− 3.32	− 3.31	0.002
				29 824	(o)	2	214.816	5.31E−05	1.36E+05	1.40E+05	− 4.03	− 4.01	0.000
				30 816	(o)	1	219.494	9.17E−05	2.35E+05	2.41E+05	− 3.77	− 3.76	0.015
				39 002	(o)	0	267.597	2.33E−01	5.96E+08	6.12E+08	− 0.19	− 0.18	0.708
				39 115	(o)	1	268.407	1.73E−01	4.44E+08	4.56E+08	− 0.32	− 0.31	0.705
				39 346	(o)	2	270.079	2.84E−01	7.28E+08	7.48E+08	− 0.10	− 0.09	0.709
				55 715	(o)	1	484.233	1.12E−06	2.88E+03	2.96E+03	− 5.00	− 4.98	0.080
				66 048	(o)	2	969.440	1.10E−05	2.83E+04	2.91E+04	− 3.40	− 3.39	0.091
				66 390	(o)	1	1002.628	2.87E−04	7.35E+05	7.55E+05	− 1.96	− 1.94	0.402
				66 493	(o)	2	1013.085	4.41E−04	1.13E+06	1.16E+06	− 1.76	− 1.75	0.319
				66 460	(o)	2	1009.706	1.72E−04	4.40E+05	4.52E+05	− 2.17	− 2.16	0.307
				67 237	(o)	0	1095.698	9.72E−04	2.49E+06	2.56E+06	− 1.35	− 1.34	0.575
				67 298	(o)	1	1103.071	6.87E−04	1.76E+06	1.81E+06	− 1.49	− 1.48	0.528
				67 396	(o)	2	1115.192	9.76E−04	2.50E+06	2.57E+06	− 1.33	− 1.32	0.472
				68 498	(o)	1	1271.473	3.72E−07	9.52E+02	9.78E+02	− 4.64	− 4.63	0.029
				75 308	(o)	2	9497.064	1.05E−07	2.69E+02	2.76E+02	− 3.44	− 3.43	0.567
				75 591	(o)	2	12 984.147	3.27E−07	8.37E+02	8.60E+02	− 2.68	− 2.66	0.581
				75 651	(o)	1	14 082.652	2.29E−07	5.87E+02	6.03E+02	− 2.76	− 2.75	0.295
				75 681	(o)	2	14 699.495	9.76E−07	2.50E+03	2.57E+03	− 2.10	− 2.08	0.578
				75 913	(o)	2	22 304.392	1.26E−08	3.22E+01	3.31E+01	− 3.64	− 3.61	0.035
				75 952	(o)	1	24 447.995	4.84E−08	1.24E+02	1.27E+02	− 2.97	− 2.94	0.375

Table 6 – *continued*

Upper level[a]			τ_u (ns)	Lower level[a]			λ^b (nm)	*BF*	gA (s^{-1})	gA_{resc} (s^{-1})	log (gf)	log $(gf)_{resc}$	CF[c]
				75 994	(o)	0	27 287.372	2.90E−08	7.44E+01	7.64E+01	− 3.11	− 3.07	0.363
				76 073	(o)	1	34 770.709	1.85E−10	4.75E−01	4.88E−01	− 5.04	− 5.05	0.031
76 589	(e)	2	1.09[e]	26 081	(o)	2	197.989	1.79E−04	7.57E+05	8.23E+05	− 3.35	− 3.32	0.040
				27 444	(o)	2	203.412	7.58E−05	3.20E+05	3.48E+05	− 3.70	− 3.67	0.170
				27 602	(o)	3	204.071	1.10E−03	4.64E+06	5.04E+06	− 2.54	− 2.50	0.490
				27 918	(o)	1	205.393	3.08E−03	1.30E+07	1.41E+07	− 2.08	− 2.05	0.390
				28 021	(o)	2	205.831	4.50E−02	1.90E+08	2.07E+08	− 0.92	− 0.88	0.454
				28 161	(o)	3	206.426	2.51E−01	1.06E+09	1.15E+09	− 0.17	− 0.13	0.529
				29 742	(o)	1	213.393	1.33E−05	5.60E+04	6.09E+04	− 4.42	− 4.38	0.000
				29 824	(o)	2	213.766	4.74E−04	2.00E+06	2.17E+06	− 2.86	− 2.83	0.001
				30 816	(o)	1	218.398	1.25E−04	5.27E+05	5.73E+05	− 3.42	− 3.39	0.012
				32 350	(o)	3	225.973	1.25E−03	5.26E+06	5.72E+06	− 2.39	− 2.36	0.328
				39 115	(o)	1	266.771	1.77E−01	7.46E+08	8.11E+08	− 0.10	− 0.06	0.705
				39 346	(o)	2	268.422	5.17E−01	2.18E+09	2.37E+09	0.37	0.41	0.709
				55 715	(o)	1	478.932	2.35E−05	9.91E+04	1.08E+05	− 3.47	− 3.43	0.019
				66 048	(o)	2	948.425	2.61E−05	1.10E+05	1.20E+05	− 2.82	− 2.79	0.065
				66 390	(o)	1	980.166	1.23E−05	5.20E+04	5.65E+04	− 3.13	− 3.09	0.219
				66 493	(o)	2	990.157	1.52E−04	6.43E+05	6.99E+05	− 2.03	− 1.99	0.337
				66 460	(o)	2	986.929	6.09E−05	2.57E+05	2.79E+05	− 2.42	− 2.39	0.243
				66 564	(o)	3	997.176	6.97E−04	2.94E+06	3.20E+06	− 1.36	− 1.32	0.372
				66 584	(o)	3	999.182	1.61E−04	6.78E+05	7.37E+05	− 1.99	− 1.96	0.215
				67 298	(o)	1	1075.944	8.96E−04	3.78E+06	4.11E+06	− 1.18	− 1.15	0.593
				67 396	(o)	2	1087.473	2.06E−03	8.71E+06	9.47E+06	− 0.81	− 0.77	0.517
				67 744	(o)	3	1130.199	9.83E−05	4.15E+05	4.51E+05	− 2.10	− 2.06	0.549
				68 498	(o)	1	1235.566	1.70E−05	7.17E+04	7.79E+04	− 2.78	− 2.75	0.138
				75 308	(o)	2	7803.238	4.76E−08	2.01E+02	2.18E+02	− 3.74	− 3.70	0.536
				75 309	(o)	3	7806.711	2.44E−07	1.03E+03	1.12E+03	− 3.03	− 2.99	0.670
				75 373	(o)	3	8220.091	2.89E−07	1.22E+03	1.33E+03	− 2.91	− 2.87	0.502
				75 552	(o)	3	9642.061	1.18E−07	5.00E+02	5.43E+02	− 3.16	− 3.12	0.304
				75 591	(o)	2	10 012.694	8.81E−09	3.72E+01	4.04E+01	− 4.26	− 4.22	0.012
				75 651	(o)	1	10 653.532	2.30E−09	9.70E+00	1.05E+01	− 4.79	− 4.75	0.011
				75 681	(o)	2	11 002.823	1.28E−07	5.40E+02	5.87E+02	− 3.02	− 2.97	0.092
				75 716	(o)	3	11 444.422	2.21E−06	9.33E+03	1.01E+04	− 1.75	− 1.70	0.611
				75 913	(o)	2	14 773.133	5.78E−07	2.44E+03	2.65E+03	− 2.11	− 2.06	0.445
				75 952	(o)	1	15 683.966	1.11E−07	4.69E+02	5.10E+02	− 2.78	− 2.73	0.354
				76 073	(o)	1	19 373.811	7.70E−09	3.25E+01	3.53E+01	− 3.73	− 3.70	0.278
77 387	(e)	3	3.73 [e]	26 081	(o)	2	194.910	2.66E−05	3.37E+04	5.00E+04	− 4.71	− 4.55	0.015
				27 444	(o)	2	200.162	8.78E−04	1.11E+06	1.65E+06	− 3.17	− 3.00	0.300
				27 602	(o)	3	200.800	2.37E−02	3.00E+07	4.45E+07	− 1.74	− 1.57	0.312
				27 841	(o)	4	201.768	2.02E−01	2.56E+08	3.80E+08	− 0.80	− 0.63	0.327
				28 021	(o)	2	202.504	1.99E−02	2.52E+07	3.74E+07	− 1.81	− 1.64	0.293
				28 161	(o)	3	203.079	1.29E−01	1.63E+08	2.42E+08	− 0.99	− 0.82	0.269
				29 824	(o)	2	210.180	1.76E−01	2.23E+08	3.31E+08	− 0.83	− 0.66	0.374
				32 350	(o)	3	221.970	4.87E−05	6.16E+04	9.14E+04	− 4.34	− 4.17	0.126
				39 346	(o)	2	262.791	1.16E−01	1.47E+08	2.18E+08	− 0.81	− 0.65	0.249
				66 048	(o)	2	881.687	2.62E−04	3.32E+05	4.93E+05	− 2.39	− 2.24	0.123
				66 493	(o)	2	917.642	8.86E−03	1.12E+07	1.66E+07	− 0.83	− 0.68	0.509
				66 460	(o)	2	914.869	6.78E−03	8.58E+06	1.27E+07	− 0.95	− 0.80	0.781
				66 564	(o)	3	923.667	6.02E−02	7.62E+07	1.13E+08	0.01	0.16	0.379
				66 584	(o)	3	925.388	7.61E−02	9.63E+07	1.43E+08	0.11	0.26	0.792
				66 719	(o)	4	937.110	1.33E−01	1.68E+08	2.49E+08	0.36	0.52	0.748
				67 396	(o)	2	1000.629	4.64E−02	5.87E+07	8.71E+07	− 0.04	0.12	0.575
				67 744	(o)	3	1036.689	4.70E−05	5.94E+04	8.81E+04	− 3.00	− 2.85	0.115
				75 221	(o)	4	4616.186	1.04E−06	1.31E+03	1.94E+03	− 3.28	− 3.21	0.152
				75 308	(o)	2	4808.601	2.30E−08	2.91E+01	4.32E+01	− 4.90	− 4.82	0.068
				75 309	(o)	3	4809.920	4.80E−08	6.07E+01	9.01E+01	− 4.58	− 4.50	0.011
				75 373	(o)	3	4963.717	4.93E−07	6.24E+02	9.26E+02	− 3.54	− 3.47	0.150
				75 390	(o)	4	5006.948	1.42E−06	1.80E+03	2.67E+03	− 3.07	− 3.00	0.104
				75 470	(o)	4	5215.252	1.24E−06	1.57E+03	2.33E+03	− 3.09	− 3.02	0.112
				75 552	(o)	3	5448.967	1.03E−06	1.30E+03	1.93E+03	− 3.13	− 3.07	0.538
				75 561	(o)	4	5474.449	1.18E−08	1.49E+01	2.21E+01	− 5.05	− 5.00	0.107
				75 591	(o)	2	5565.388	5.53E−07	7.00E+02	1.04E+03	− 3.37	− 3.32	0.306

Table 6 – *continued*

Upper level[a]	τ_u (ns)	Lower level[a]			λ^b (nm)	*BF*	*gA* (s^{-1})	gA_{resc} (s^{-1})	log (*gf*)	log $(gf)_{resc}$	CF[c]
		75 681	(o)	2	5858.418	1.88E−06	2.38E+03	3.53E+03	− 2.79	− 2.74	0.571
		75 716	(o)	3	5981.306	1.01E−05	1.28E+04	1.90E+04	− 2.04	− 1.99	0.848
		75 913	(o)	2	6779.698	4.40E−07	5.56E+02	8.25E+02	− 3.28	− 3.24	0.072

Notes. [a]Each level is designated by its value in cm^{-1}, its parity ((e) and (o) stand for even and odd, respectively) and its total quantum number, *J*.
[b]Calculated from the energy levels compiled by NIST (Kramida et al. 2015). $\lambda > 200$ nm are given in air.
[c]Cancellation factor as defined by Cowan (1981). A value less than 5 per cent indicates a strong cancellation effect on the line strength and the transition probability could be underestimated.
[d]TR-LIF measurements by Marsden et al. (1988).
[e]TR-LIF measurements, this work.

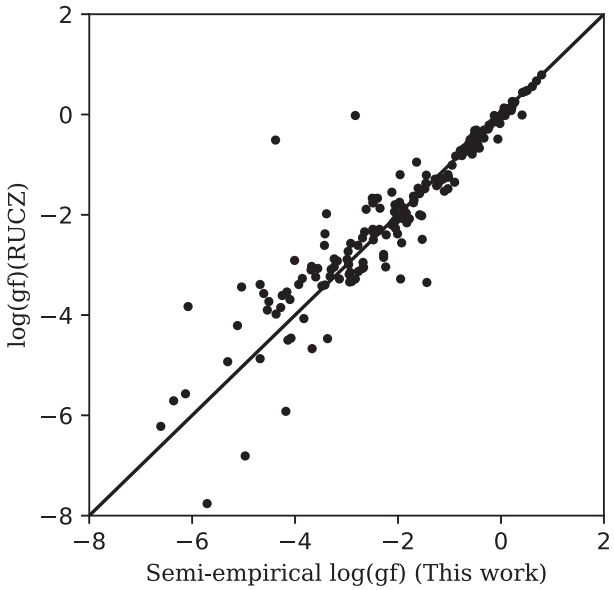

Figure 4. A comparison between the oscillator strengths determined by the combination of the HFR+CPOL branching fractions and the TR-LIF lifetimes (this work) and the semi-empirical oscillator strengths calculated by Ruczkowski et al. (2014) (RUCZ). The straight line of equality has been drawn.

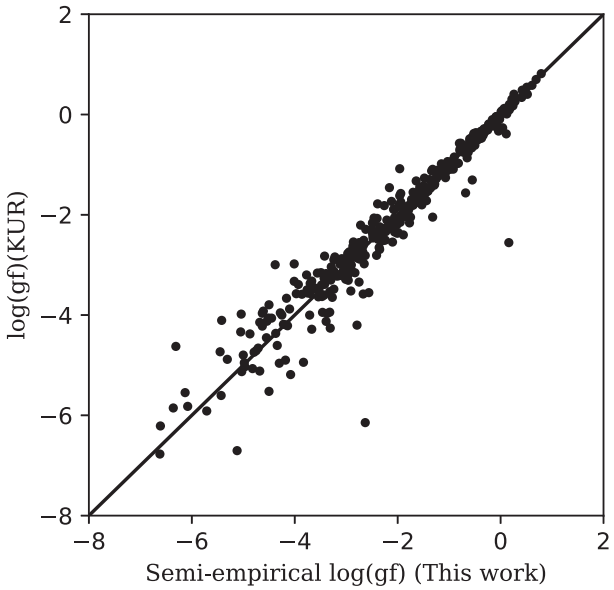

Figure 5. A comparison between the oscillator strengths determined by the combination of the HFR+CPOL branching fractions and the TR-LIF lifetimes (this work) and the oscillator strengths calculated by Kurucz (2011) (KUR). The straight line of equality has been drawn.

the meteoritic abundances (Lodders et al. 2009) still remains for scandium with $\log \epsilon_{\odot} = 3.16 \pm 0.04$ and $\log \epsilon_{met} = 3.05 \pm 0.02$.

The Sc II lines used in Scott et al. (2015) for the determination of the solar abundance of scandium are presented in Table 7. These lines are from low-excited levels measured by Lawler & Dakin (1989) but not included in this study. The third column of this table contains the oscillator strengths deduced from the *A*-values of Lawler & Dakin (1989) used by Scott et al. (2015) to determine the photospheric abundances listed in the sixth column. They are compared to our rescaled oscillator strengths reported in the fourth column and the differences between the two values are given in the log scale in the fifth column. For this set of solar lines, our oscillator strengths are systematically larger than those of Lawler & Dakin (1989) by ∼0.1 dex on average, if we exclude the transition $3d^2\ ^1D_2 - 3d4p\ ^1D^o_2$ for which our *f*-value is affected by strong cancellation effects. Column seven in Table 7 gives the abundances obtained from each line, assuming they are all lying on the linear part of the curve of growth (see the upper left panel of fig. 3 in Scott et al. (2015)), with our new *gf*-values.

The weighted average along with the corresponding weighted standard deviation of the abundance was determined using the weights of Scott et al. (2015), reported in the last column of Table 7. Their weights range from one to three and are based on the line quality for abundance determination. Discarding the line $3d^2\ ^1D_2 - 3d4p\ ^1D^o_2$ from the mean estimate, one obtains $\log \epsilon_{cor} = 3.04 \pm 0.13$ (where the second number is the standard deviation) for the corrected photospheric abundance, now in good agreement with the meteoritic value of Lodders et al. (2009). Even if we reject the transition $3d^2\ ^3F_4 - 3d4p\ ^3F^o_3$ for which there is a factor of two difference between our rescaled *f*-value and the experimental value of Lawler & Dakin (1989), the mean $\log \epsilon_{cor} = 3.10 \pm 0.05$ is still in accord with the meteoritic value. Moreover, considering the full line set does not change the agreement ($\log \epsilon_{cor} = 3.07 \pm 0.17$). Finally, we note that all these weighted average abundances agree within the mutual error bars with the value determined by Scott et al. (2015) using only Sc I lines ($\log \epsilon = 3.14 \pm 0.09$).

Replacing our *f*-value set by the one of Kurucz (2011) will not change this accord either ($\log \epsilon_{kur} = 3.10 \pm 0.09$). This is not the case for the set of Ruczkowski et al. (2014). Indeed, the photospheric abundance would be estimated significantly too high with respect to the meteoritic value, i.e. $\log \epsilon_{ruc} = 3.44 \pm 0.31$. Even if the transition $3d^2\ ^3F_4 - 3d4p\ ^3F^o_3$ for which the oscillator strength calculated by Ruczkowski et al. (2014) ($\log (gf)_{ruc} = -3.28$) is one order of magnitude lower than the experimental value of Lawler &

Table 7. Sc II lines used in the determination of the solar abundance ($\log \epsilon$) of scandium.

Transition			λ^a (nm)	$\log(gf)^b_{\rm L\&D}$	$\log(gf)^c_{\rm resc}$	$\Delta\log(gf)^d$	$\log\epsilon^e$	$\log\epsilon^f_{\rm cor}$	Weight^e
$3d^2\,{}^3F_4$	–	$3d4p\,{}^3F^o_3$	442.067	−2.273	−1.950	0.323	3.099	2.776	2
$3d^2\,{}^3F_3$	–	$3d4p\,{}^3F^o_2$	443.135	−1.969	−1.780	0.189	3.155	2.966	1
$3d^2\,{}^3P_2$	–	$3d4p\,{}^1P^o_1$	535.720	−2.111	−2.050	0.061	3.131	3.070	2
$3d^2\,{}^3P_1$	–	$3d4p\,{}^3P^o_2$	564.100	−1.131	−1.000	0.131	3.226	3.095	1
$3d^2\,{}^3P_0$	–	$3d4p\,{}^3P^o_1$	565.836	−1.208	−1.150	0.058	3.211	3.153	1
$3d^2\,{}^3P_1$	–	$3d4p\,{}^3P^o_1$	566.715	−1.309	−1.220	0.089	3.235	3.146	1
$3d^2\,{}^3P_1$	–	$3d4p\,{}^3P^o_0$	566.904	−1.200	−1.100	0.100	3.246	3.146	1
$3d^2\,{}^3P_2$	–	$3d4p\,{}^3P^o_1$	568.420	−1.074	−1.030	0.044	3.154	3.110	2
$3d^2\,{}^1D_2$	–	$3d4p\,{}^1D^o_2$	660.460	−1.309	−1.570^g	−0.261	3.204	3.465	1

Notes. [a]Calculated from the energy levels compiled by NIST (Kramida et al. 2015).
[b]Scott et al. (2015), deduced from the *A*-values of Lawler & Dakin (1989).
[c]This work, rescaled value.
[d]$\Delta\log(gf) = \log(gf)_{\rm L\&D} - \log(gf)_{\rm resc}$.
[e]Scott et al. (2015).
[f]This work, corrected abundance, $\log\epsilon_{\rm cor} = \log\epsilon - \Delta\log(gf)$.
[g]Affected by strong cancellation effects ($CF < 0.05$).

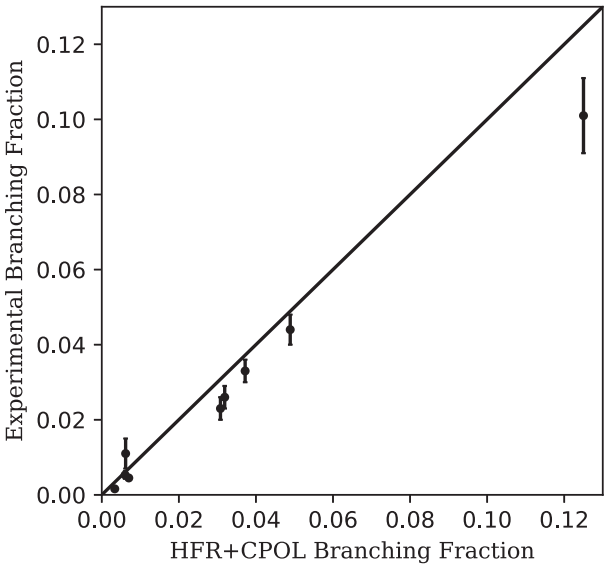

Figure 6. A comparison between the HFR+CPOL branching fractions and the experimental values of Lawler & Dakin (1989) for the Sc II lines used in the determination of the solar scandium abundance. The straight line of equality has been drawn.

Dakin (1989) is excluded, this would not significantly improve the situation ($\log\epsilon_{\rm ruc} = 3.29 \pm 0.01$).

It should be noted, however, that the lines used for these studies are weak, see Fig. 6. Their *BFs* are less than 5 per cent except for λ566.904 having ∼10 per cent. These small *BFs* make it difficult to measure and calculate with high accuracy. The real uncertainty might thus be larger than the observed scatter.

7 CONCLUSIONS

New TR-LIF lifetimes were measured using two-step excitation schemes in Sc II. These measurements extend the set of available experimental values with 17 even-parity levels belonging to the excited configurations 3d5s, 3d4d, $4p^2$ and 3d6s. We measured 57 *BFs* from these upper levels using an HCL and an FTS. By combining the *BFs* with the measured lifetimes, we derived $\log(gf)$ values from these highly excited levels. A HFR model that includes the main relativistic interactions along with the core-polarization effects (HFR+CPOL) was used to determine the branching fractions and the oscillator strengths. The comparison between our HFR+CPOL and TR-LIF lifetimes along with those found in the literature (Buchta et al. 1971; Arnesen et al. 1976; Palenius et al. 1976; Vogel et al. 1985; Marsden et al. 1988; Kurucz 2011; Ruczkowski et al. 2014) shows generally a good agreement ranging from a few per cent to 20 per cent with the notable exceptions of the even-parity levels $4p^2\,{}^1D_2$ and $3d6s\,{}^3D_3$. The former discrepancy may be due to a cancellation effect that lengthens the HFR+CPOL lifetime. Owing to the good agreement (∼20 per cent) obtained with the experimental branching fractions of Lawler & Dakin (1989) for low-excitation levels and ours for high-excitation levels, the HFR+CPOL branching fractions were combined with our TR-LIF lifetimes and the experimental values of Marsden et al. (1988) to obtain rescaled semi-empirical oscillator strengths for all the 380 E1 transitions depopulating the 34 fine-structure levels for which TR-LIF lifetimes are available. This new set of oscillator strengths was compared to the parametric calculation of Ruczkowski et al. (2014) and to the HFR values of Kurucz (2011). In both cases, the mean scatters were ∼20 per cent for the strong lines ($\log(gf) \gtrsim -1$) giving an estimate of the accuracy for these radiative parameters. Finally, the solar abundance of scandium was estimated to $\log\epsilon_\odot = 3.04 \pm 0.13$ using our rescaled semi-empirical oscillator strengths to correct the values determined in the recent study of Scott et al. (2015). This value is in improved agreement with the meteoritic value ($\log\epsilon_{\rm met} = 3.05 \pm 0.02$) of Lodders et al. (2009).

ACKNOWLEDGEMENTS

This work was financially supported by the Integrated Initiative of Infrastructure Project LASERLAB-EUROPE, contract LLC002130 and the Belgian FRS-FNRS. PQ and PP are Research Director and Research Associate of the FRS-FNRS, respectively. We acknowledge the support from the Swedish Research Council through a Linnaeus grant to the Lund Laser Centre and through project grant 2016-04185, as well as the Knut and Alice Wallenberg Foundation. MTB, JCP and CC thank the STFC (UK) for support of their Laboratory Astrophysics research at Imperial College London. VF is currently a post-doctoral researcher of the Return Grant programme of the Belgian Scientific Policy (BELSPO). The Belgian team is grateful to the Swedish colleagues for the warm

hospitality enjoyed at the Lund Laser Centre during the two campaigns of measurements performed in 2015 June and August.

REFERENCES

Arnesen A., Bengtsson B., Curtis L. J., Hallin R., Nordling C., Noreland T., 1976, Phys. Lett., 56A, 355
Buchta R., Curtis L. J., Martinson I., Brzozowski J., 1971, Phys. Scr., 4, 55
Cowan R. D., 1981, The Theory of Atomic Structure and Spectra. University of California Press, Berkeley
Davis S. P., Abrams M. C., Brault J. W., 2001, Fourier Transform Spectrometry. Academic Press, San Diego
Engström L., 1998, Technical Report LRAP-232, A Computer Program to Determine Peak Positions and Intensities in Experimental Spectra. Atomic Physics, Lund Univ., Lund, Sweden
Engström L., 2014, GFit. Available at: http://kurslab-atom.fysik.lth.se/Lars/GFit/Html/index.html
Engström L., Lundberg H., Nilsson H., Hartman H., Bäckström E., 2014, A&A, 570, A34
Johansson S., Litzén U., 1980, Phys. Scr., 22, 49
Johnson W. R., Kolb D., Huang K.-N., 1983, Atom. Dat. Nucl. Dat. Tables, 28, 333
Kramida A., Ralchenko Yu., Reader J., NIST ASD Team, 2015, http://physics.nist.gov/asd (accessed 2015 August 17)
Kurucz R. L., 2011, http://kurucz.harvard.edu/atoms.html (accessed 2015 August 17)
Lawler J. E., Dakin J. T., 1989, J. Opt. Soc. Am., 6, 1457
Lind K., Bergmann M., Asplund M., 2012, MNRAS, 427, 50
Lodders K., Palme H., Gail H.-P., 2009, in Trümper J. E., ed., Landolt Börnstein, New Series, Vol. VI/4B, Chap. 4.4, Abundances of the Elements in the Solar System, Springer-Verlag, Berlin, p. 560
Lundberg H. et al., 2016, MNRAS, 460, 356
Marsden G. C., Den Hartog E. A., Lawler J. E., Dakin J. T., Roberts V. D., 1988, J. Opt. Soc. Am., 5, 606
Neufeld L. W., 1970, Dissertation, Kansas State Univ.
Pagel E. B. J., 2009, Nucleosynthesis and Chemical Evolution of Galaxies. Cambridge Univ. Press, Cambridge
Palenius H. P., Curtis L. J., Lundlin L., 1976, J. Phys. B, 9, L473
Palmeri P., Quinet P., Fivet V., Biémont E., Nilsson H., Engström L., Lundberg H., 2008, Phys. Scr., 78, 015304
Pehlivan A., Nilsson H., Hartman H., 2015, A&A, 582, A98
Pickering J. C., 2002, Vib. Spectrosc., 29(1,2), 27
Quinet P., Palmeri P., Biémont E., McCurdy M. M., Rieger G., Pinnington E. H., Wickliffe M. E., Lawler J. E., 1999, MNRAS, 307, 934
Ruczkowski J., Elantkowska M., Dembczynski J., 2014, J.Q.S.R.T., 145, 20
Russell H. N., Meggers W. F., 1927, Sci. Papers Natl. Bur. Stand. (U.S.), 22, 329
Scott P., Asplund M., Grevesse N., Bergemann M., Sauval A. J., 2015, A&A, 573, A26
Sikström C. M., Nilsson H., Litzen U., Blom A., Lundberg H., 2002, J. Quant. Spectr. Rad. Transf., 74, 355
Vogel O., Ward L., Arnesen A., Hallin R., Nordling C., Wannstrom A., 1985, Phys. Scr., 31, 166

This paper has been typeset from a TEX/LATEX file prepared by the author.